Journal of Physical Chemistry A
Submission Closing Date 31 March 2021
Submitted March 30, 2021
Revised April 30, 2021

# The Chemical Bonding and Electronic Structure of the Early Transition Metal Borides: ScB, TiB, VB, YB, ZrB, NbB, LaB, HfB, TaB, and WB[†]

Dakota M. Merriles, Christopher Nielson, Erick Tieu, and Michael D. Morse[*]
Department of Chemistry
University of Utah
Salt Lake City, UT 84112

[†]Submitted as part of the "Alexander Boldyrev Festschrift"

[*] Corresponding author. E-mail: morse@chem.utah.edu

**ABSTRACT:**

The predissociation thresholds of the early transition metal boride diatomics (MB, M = Sc, Ti, V, Y, Zr, Nb, La, Hf, Ta, W) have been measured using resonant two-photon ionization (R2PI) spectroscopy, allowing for a precise assignment of the bond dissociation energy (BDE). No previous experimental measurements of the BDE exist in the literature for these species. Owing to the high density of electronic states arising from the ground and low-lying separated atom limits in these open d-subshell species, a congested spectrum of vibronic transitions is observed as the energy of the ground separated atom limit is approached. Nonadiabatic and spin-orbit interactions among these states, however, provide a pathway for rapid predissociation as soon as the ground separated atom limit is reached, leading to a sharp decrease in signal to background levels when this limit is reached. Accordingly, the BDE's of the early transition metal borides have been assigned as: $D_0$(ScB): 1.72(6) eV, $D_0$(TiB): 1.956(16) eV, $D_0$(VB): 2.150(16) eV, $D_0$(YB): 2.057(3) eV, $D_0$(ZrB): 2.573(5) eV, $D_0$(NbB): 2.989(12) eV, $D_0$(LaB): 2.086(18) eV, $D_0$(HfB): 2.593(3) eV, $D_0$(TaB): 2.700(3) eV, and $D_0$(WB): 2.730(4) eV. Additional insight into the chemical bonding and electronic structure of these species has been achieved by quantum chemical calculations.

## 1. INTRODUCTION

In all disciplines of chemistry, the chemical bond is of the greatest relevance. Indeed, the process of breaking chemical bonds and forming new ones defines a chemical reaction. There is no other measurement of a chemical bond that is as fundamental as the bond dissociation energy (BDE), the amount of energy needed to take a molecule in its ground vibronic state to its ground separated atom limit. BDEs are universally employed to compare the strength of chemical bonds, to derive reaction enthalpies, and to develop a chemical understanding of the bonding in specific molecules. Ultimately, accruing insight into the bond between two atoms can be quantitatively achieved by measuring the BDE.

Not only is the BDE an extremely important quantifier of the chemical bonding in a molecule, the BDE also participates in various thermochemical cycles that can be employed to obtain additional relevant information for a molecule. A highly useful thermochemical cycle for a diatomic molecule, AB, relates the molecule's BDE in its neutral and singly ionized forms, the ionization energy of atom A, and the ionization energy of the molecule itself. Here, the same amount of energy is required to dissociate the neutral molecule and subsequently ionize atom A as is required to ionize the molecule and then dissociate the cationic species:

$$D_0(AB) + IE(A) = IE(AB) + D_0(A^+\text{-}B)\,. \tag{1.1}$$

In this equation, $D_0(AB)$ is the energy required to take the AB molecule in its ground state to its ground separated atom limit, IE(A) is the ionization energy of atomic species A, $D_0(A^+\text{-}B)$ is the cationic analog to $D_0$, and IE(AB) is the ionization energy of the molecule, AB. Another important thermochemical cycle relates the BDE to the gaseous enthalpy of formation of a molecule at 0 K:

$$\Delta_f H^0_{0K}(AB_{(g)}) = \Delta_f H^0_{0K}(A_{(g)}) + \Delta_f H^0_{0K}(B_{(g)}) - D_0(AB). \tag{1.2}$$

Here $\Delta_f H^0_{0K}(AB_{(g)})$ is the standard enthalpy of formation of the gaseous diatomic molecule AB at 0 K; $\Delta_f H^0_{0K}(A_{(g)})$ and $\Delta_f H^0_{0K}(B_{(g)})$ are the gaseous enthalpies of formation of atomic species A and B at 0 K, respectively; and $D_0(AB)$ is the 0 K BDE of the AB molecule. The quantities described in Eqns 1.1 and 1.2 can further be related to a molecule's electron affinity, anionic dissociation energy, *etc*., in other thermochemical cycles.

These thermochemical cycles, particularly that described by Eqn. 1.1, allow for a strict confirmation of self-consistency when all the values that participate in the thermochemical cycle are independently known. Studies on $V_2$ and LaSi demonstrate the agreement that should be found when thermochemical quantities are rigorously checked for consistency. The ionization energies of V and $V_2$ have been precisely measured using Rydberg extrapolation and PFI-ZEKE spectroscopy, giving 6.746187(21) eV and 6.356814(62) eV, respectively.[1, 2] The BDEs of $V_2$ as a neutral and singly ionized species have been measured by the observation of a sharp predissociation threshold in a congested electronic spectrum, giving 2.752(1) eV and 3.140(2) eV, respectively.[3, 4] The two sides of Eqn. 1.1 for $V_2$, calculated from completely independent measurements, agree to within 0.0019(21) eV. This shows an exceptionally high level of consistency between the four measurements. The same standard of consistency epitomized by $V_2$ can also be demonstrated with LaSi. The BDE of the neutral LaSi molecule has been measured using R2PI spectroscopy to be 2.891(5) eV.[5] The observation of two Rydberg series in La was used to deduce IE(La) = 5.5769(6) eV.[6, 7] An experimental measurement of 2.87(10) eV for $D_0(La^+\text{-Si})$ has been obtained from Guided Ion Beam Mass Spectrometry (GIBMS).[8] By inserting these values into Eqn. 1.1, the ionization energy of LaSi can be

calculated to be 5.60(10) eV, which is in excellent agreement with an experimental measurement of IE(LaSi) obtained using R2PI spectroscopy, 5.613(11) eV.[5]

In both of these demonstrations of thermochemical self-consistency, R2PI spectroscopy was used to measure the BDE of the neutral species. The BDEs were assigned from the observation of a sharp predissociation threshold in a congested spectrum of vibronic transitions as the ground separated atom limit of the species was approached. Above the ground separated atom limit, the molecule is strongly perturbed by a dense manifold of vibronic states, and prompt dissociation readily occurs at threshold through nonadiabatic and/or spin-orbit coupling to states that dissociate to ground state atoms. Thus, the observation of a sharp predissociation threshold can be used to assign the BDE for a molecule with R2PI spectroscopy. This technique has been previously employed to precisely measure the BDEs for transition metal boride,[9] aluminide,[10, 11] carbide,[5, 12-15] silicide,[5, 14, 16, 17] nitride,[12] oxide,[18] sulfide,[12-14, 19-21] selenide,[13, 14, 21-23] and chloride[14] diatomics. In this article, we report ten highly precise BDEs for early transition metal borides using the same spectroscopic method.

Early transition metal-boron containing compounds have been found to exhibit an impressive array of physiochemical properties. The superconductivity of various transition metal borides, such as $MgB_2$ and $FeB_4$, is well established.[24, 25] Recently, solid $MRh_2B_2$ (M = Nb, Ta) compounds have been found to be superconductors with a chiral, noncentrosymmetric crystal structure, a unique departure from the inversion symmetry that is exhibited in the majority of superconductor crystal structures.[26] The high hardness, electrical conductivity, and thermal stabilities of early transition metal boride materials in thin films and ultra-high temperature ceramics have also been well studied.[27-30] The intrinsic physicochemical properties demonstrated by these compounds have naturally led to theoretical studies that aim to predict even more

properties of transition metal borides for uses in a wide variety of disciplines.[31-36] The electronic structure and BDEs of diatomic transition metal borides have also been the focus of computational studies.[37-41]

Prior to the present study, no experimental BDE measurements had been reported for the early transition metal boride diatomics. In contrast to other early transition metal-p-block bonds, the early transition metal-boron bond is severely understudied in the gas phase.[42] Experimentally derived values of the ground electronic configurations and terms, bond lengths, harmonic frequencies, and BDEs for the early transition metal MB species are completely unknown. Commonly reported BDEs, estimated using the Pauling Method for ScB and TiB, have error limits as large as 20% of the reported value.[43] An error limit this large nearly precludes an elucidation of the bonding trends in these species. Further, it is far too large to be used as a test of whether computations on transition metal borides reach "experimental accuracy," a term that was first defined as 1 kcal $mol^{-1}$ by John Pople in his Nobel lecture.[44] For transition metal containing species, experimental accuracy has been relaxed to 3 kcal $mol^{-1}$ because of the inherent challenges related to quantum calculations on systems that involve highly correlated electrons, strong spin-orbit interactions, and significant relativistic effects.[45] Theoretical and computational chemists commonly lament that stringent benchmarks, in particular BDEs, that can achieve experimental accuracy standards to test quantum calculation methods for these early MB species are needed because none exist.[37-39, 46, 47] In the present study, BDEs for early MB species have been precisely measured and are available to be used as rigorous benchmarks for quantum calculation methods. Additionally, together with the periodic bonding trends for the late MB species,[9] a quantitative and qualitative landscape of the chemical bond between a transition metal and boron can be established.

## 2. EXPERIMENTAL SECTION

R2PI spectroscopy was performed on the early MB molecules using the same instrumentation as in previous BDE experiments on the late transition metal borides and the FeX, and NiX (X=C, S, Se) species.[9, 13] In these experiments, the diatomic molecules of interest are produced in a stainless steel reaction block with intersecting, perpendicular channels. The longer channel runs the length of the reaction block and terminates in a low-pressure chamber, while the shorter channel traverses the width of the reaction block. The distance from the channel intersection to the terminating orifice of the longer channel is termed the reaction channel. A pulse of high-pressure helium carrier gas (5-30 psi) enters the longer channel as a coincident pulse of fundamental radiation (5ns, 1064nm, ≈30mJ) from a pulsed Nd:YAG laser traverses the shorter channel and vaporizes a rotating and translating metal disk placed at the end of the channel. The focused Nd:YAG fundamental radiation ablates the metal surface, ejecting a gaseous plasma of metal atoms, ions, and electrons. The metal samples used in this study were all pure metal samples (Ti, Y, Zr, Nb, La, Hf, Ta, W) except in the cases of Sc and V where Sc:Cu (1:1) and V:Ta (4:1) alloys were used. This was simply for convenience because these samples were available in the laboratory. The timing between the carrier gas pulse and the ablation of the metal sample is optimized so that the ablated metal atoms enter the channel intersection while the gas pulse is present. The gaseous plasma is entrained into the helium carrier gas and begins flowing down the reaction channel. To produce the early transition metal boride species in this study, reactant diborane gas is seeded (0.03% - 0.12%) into the helium carrier gas and reacts with the gaseous plasma in the reaction channel. The diborane used in these experiments was purchased as a 5% mixture in hydrogen, but was purified to eliminate the hydrogen as previously described.[9]

In contrast to our studies of the late transition metal borides, the production of the early transition metal borides was greatly enhanced by lower concentrations of diborane seeded in helium. When higher concentrations were used, large numbers of $M_xB_y$ (x=1-6, y=2-8) clusters were readily formed, reducing the production of the desired transition metal monoboride molecules. Likewise, unfavorable metal boride cluster production was highly exacerbated when longer reaction channels were installed. These increased the reaction time prior to expansion, allowing the production of larger metal boride clusters. Production of the early monoboride diatomic molecules of interest was greatly improved by using short reaction channels to reduce the reaction time.

Even though the production of $M_xB_y$ clusters could be adequately minimized, the production of $MB_2$ species was nearly impossible to circumvent. This observation can be rationalized with a rudimentary understanding of the bonding in $MB_2$ molecules *vs.* the bonding in MB molecules. The electron affinity of $B_2$ is about seven times larger than the electron affinity of B.[48-50] A likely ramification of this fact is the much more electropositive early transition metals can form thermochemically stable diboride species *via* a donation of electrons from the early transition metals to the $B_2$ unit that is already present in diborane. Experimental BDEs of UB and $UB_2$ from Knudsen effusion mass spectrometry support this idea: the reported bond strength of $UB_2$ is twice that of its monoboride counterpart.[51] In the investigation of LaB's predissociation threshold, the signal due to $LaB_2$ dominated the LaB ion signal, regardless of the reaction conditions employed. A different approach of aggressively rubbing our La sample in isotopically pure $^{11}B$ powder to try to produce LaB upon sample surface ablation was inspired by the success of an analogous procedure for R2PI on NaAg and NiSi.[52, 53] Using helium carrier gas and ablating the La sample surface coated in $^{11}B$ powder resulted in the LaB signal dominating the $LaB_2$ signal, a

huge improvement over trying to produce LaB by reacting La with various concentrations of diborane. In short, the optimal reaction conditions for early MB production were those which minimized the production of $M_xB_y$ clusters and $MB_2$.

Based on previous spectroscopic experiments in the group, the reaction products are generally cooled to a temperature that is close to ambient *via* numerous collisions with helium carrier gas in the reaction channel. The rotational degrees of freedom are then further cooled through supersonic expansion as the molecules exit the high-pressure reaction channel into a low-pressure chamber ($10^{-5}$ Torr). It is estimated that the rotational temperature of the hottest molecules in the molecular beam is no more than 30 K.[54, 55] After exiting the reaction channel, the expanding free jet continues downstream where it is roughly collimated by passage through a 1 cm diameter conical skimmer and enters a second low pressure chamber ($10^{-6}$ Torr) that houses a Wiley-McLaren time-of-flight electrode assembly.[56] Within the electrode assembly, the molecular beam is first irradiated with photons from a tunable optical parametric oscillator (OPO) laser. This promotes the molecules to an excited state when the photon energy matches the energy of an allowed spectroscopic transition. Then, 20 nanoseconds after excitation, the excited molecules are carried to the ionization continuum by irradiation with the 5$^{th}$ harmonic (5.83 eV) of a pulsed Nd:YAG laser. In the experiment on LaB, the 4$^{th}$ harmonic radiation (4.66 eV) was used instead, as the 5ω radiation was sufficient to one-photon ionize the molecule, violating the conditions required for R2PI spectroscopy. Once ionized, the species are accelerated by the Wiley-McLaren electrode assembly up the drift tube of a time-of-flight mass spectrometer. Here, the species in the molecular beam separate by mass and eventually impact a dual microchannel plate detector. The resulting voltage waveform is preamplified, digitized, and recorded using a personal computer. The temporal separation of the mass peaks in the digitized waveform permits

mass-specific optical spectra of several masses to be collected simultaneously as a function of tunable laser wavelength. The experimental cycle operates at a 10 Hz repetition rate.

In these experiments, the OPO laser is scanned from lower to higher energies, and 30 shots are averaged at each wavelength increment. Once the predissociation threshold of the molecule is observed, numerous scans about the threshold are averaged for the assignment of the bond dissociation energy. The R2PI spectrum of the transition metal constituent is recorded simultaneously with the molecule of interest for the purpose of observing atomic transitions. These are then matched to known atomic transitions from NIST in order to calibrate the spectra.[7] In unfortunate cases where there are insufficient assignable atomic transitions near the predissociation threshold, another transition metal or lanthanide sample is subsequently installed and used for the calibration.

As one approaches the energy of the ground separated atom limit in these molecules, the R2PI spectra become dense and, in many cases, quasicontinuous due to the high density of electronic states that are present. Electronic states correlating to the ground separated atom limit are supplemented in this region by states arising from higher lying limits. Bound states that correlate to the higher limits are probably the source of favorable Franck-Condon factors that allow spectroscopic excitation to occur near the ground separated atom limit. These bound states are coupled to dissociative states by nonadiabatic and spin-orbit interactions, however, which facilitate rapid predissociation when the ground separated atom limit is reached or exceeded. When the molecule predissociates before it can be ionized by the second laser pulse, the ion signal drops to baseline, allowing the BDE to be measured.

For some of the molecules investigated here, discrete features were observed in the spectra that then disappeared at higher energies as predissociation set in. To investigate whether

these discrete states could be predissociating but at a slower rate, time-delayed R2PI was used to measure the lifetime of the excited state. In this method, the molecule is excited by the OPO laser, and the ionization laser is fired after a variable time delay. The ion signal is then monitored as a function of the delay, giving an exponential decay curve. By fitting the exponential decay, the 1/e lifetime of the excited state could be extracted and compared to that of lower energy states that were apparently below the predissociation threshold.

It should be noted that the signal intensities for these early transition metal monoborides were generally quite weak compared to other species we have investigated by this technique. It was generally not possible to make these molecules in the same quantities as other species we have studied. This is undoubtedly due to the relatively weak MB bonds in these species, combined with the need to go to low diborane concentrations and short reaction times in order to minimize interference from the more strongly bound $MB_2$ molecules and larger clusters. In addition, the structured spectra that were obtained for some of the molecules necessitated somewhat larger error limits than we have reported in our previous BDE measurements.

## 3. COMPUTATIONAL DETAILS

All of the density functional theory (DFT) calculations in this work were performed using the Gaussian16 software suite.[57] The unrestricted B97-1 density functional method[58] was employed for these calculations. It has been reported that the B97 functional displays the highest level of accuracy when used to benchmark the BDEs of transition metal containing diatomics.[59] Diffuse-augmented correlation-consistent basis sets of triple-zeta quality were used for Y, Zr, Nb, La, Hf, Ta, W (aug-cc-pVTZ-PP)[60-63] and a correlation-consistent basis set of triple-zeta

quality was used for B (cc-pVTZ)[64] in all calculations. The energy-consistent relativistic pseudo-potentials developed by the Stuttgart-Cologne group were applied to Y, Zr, Nb (ECP28MDF)[60], La (ECP46MWB)[63, 65], and Hf, Ta, W (ECP60MDF)[66]. Geometry optimizations and time-dependent density functional theory (TD-DFT) excited state calculations were performed to elucidate the ground electronic configurations and spin multiplicities of the early 4d and 5d-MB species. The MB's were calculated with spin multiplicities that correspond to their transition metal constituent in its $s^2d^n$ and $s^1d^{n+1}$ configurations bonded to boron in its ground doublet spin multiplicity. YB and LaB were calculated with singlet, triplet, and quintet multiplicities. ZrB and HfB were calculated with doublet, quartet, and sextet multiplicities. NbB and TaB were calculated with triplet, quintet, and septet multiplicities. WB was calculated with quartet, sextet, and octet multiplicities. The ground state energies of all of the transition metals and boron were separately computed for bond dissociation energy calculations.

## 4. RESULTS

The R2PI spectra of ScB, TiB, VB, YB, ZrB, NbB, LaB, HfB, TaB, and WB in the vicinity of their predissociation thresholds are displayed in Figures 1-10, respectively. In these figures, the top trace provides the recorded molecular signal of the MB molecule; the atomic transitions that were used for calibration are shown in the lower trace(s). The arrow displayed in each figure indicates the assigned BDE of the molecule, while the bar atop the arrow represents the assigned error limit.

The error limits assigned for the BDEs of these early transition metal borides are largely based on the appearance of the predissociation threshold. For ScB, VB, and LaB, discrete features persisted above what appeared to be the predissociation threshold. For these features, time-

delayed R2PI methods were used to measure the 1/e decay time of the excited state, which was compared to the lifetimes of states that clearly lie below the predissociation threshold. In all cases, the lifetimes of the high-energy discrete states were similar to the lower energy states, giving no suggestion that the high-energy discrete states were undergoing predissociation. Accordingly, the predissociation threshold in these cases was assigned at the last of the discrete features, with an error limit sufficient to encompass the spacing between discrete features.

For ZrB and NbB, a gradual decrease in molecular signal was observed in the R2PI spectra as the predissociation threshold was approached from below. This is most likely the result of poor Franck-Condon overlap with the spectroscopically accessible states in this region, preventing a sharp drop in molecular signal as the bond dissociation energy is exceeded. In these cases, a slightly larger error limit was assigned to compensate for the somewhat ambiguous predissociation thresholds. In contrast, the predissociation thresholds of YB, HfB, and TaB are good examples of sharp, clearly defined predissociation thresholds separating a quasi-continuous spectrum from baseline. As a result, a small error limit of ±25 $cm^{-1}$ could be assigned for all three of these BDEs. The assigned error limits for these measurements also account for experimental uncertainties such as broadening of the threshold due to the finite rotational temperature of the molecules (≈20 $cm^{-1}$) and the linewidth of the OPO laser (≈10 $cm^{-1}$).[54, 55]

In the R2PI spectrum of YB, displayed in Figure 4, the molecular signal crashes to baseline prematurely near 16150 $cm^{-1}$. This interruption of the YB molecular signal is a result of the strongly allowed $4d^1\ 5s^1\ 5p^1$, $^2D°_{5/2,\ 3/2} \leftarrow 4d^1\ 5s^2$, $^2D_{3/2}$ transitions in atomic yttrium.[7] At the wavenumbers of these transitions, an overwhelming number of $^{89}Y^+$ ions are created in the ion source. The large number of $Y^+$ ions causes the ion cloud to expand so severely as it travels up the flight tube that the majority of ions of all types miss the detector. The signal of the atomic

$^{89}Y^+$ ions remains quite intense, however, because the number of atomic ions produced is so enormous. In contrast, the expansion of the ion cloud causes all other species in the beam to be highly depleted at these wavelengths. Moreover, the $^{89}Y^+$ signal at these transitions is so intense that the time-of-flight waveform for the atom displays ringing that extends into the YB mass channel, also contributing to the loss of YB signal. Similarly, there is also a dip in the baseline signal at 21534 $cm^{-1}$ in the R2PI spectrum of ZrB, shown in Figure 5. This is an artifact of an intense ZrO transition at this wavenumber that caused the background ZrB signal to disappear entirely. A similar effect is also seen in the R2PI spectrum of TaB, shown in Figure 9, where there is a slight bump in the baseline signal at 21855 $cm^{-1}$. The artificial increase in TaB molecular signal here is from the waveform of the strongly allowed $^{181}Ta$ transition at 21855 $cm^{-1}$ ringing into the mass channel for TaB. Unlike the negative-going ring that led to an artificial drop in YB signal, a positive phase of the ringing led to an artificial amplification of the TaB molecular signal. In all of these examples, these artificial changes in molecular signal are well-understood artifacts, similar to ones that have been previously observed.[5, 9]

## 5. DISCUSSION

### A. The 3d Early Transition Metal Borides: ScB, TiB, and VB

The molecular orbital (MO) diagram of the early transition metal borides is similar to the corresponding MO diagram of the late transition metal borides. A qualitative depiction of the MO diagram for the early MB species is displayed in Figure 11 based on a DFT calculation on LaB, as described in Section III. The pertinent bonding, nonbonding, and antibonding orbitals for the early MB species are generated from the valence (n+1)s and nd atomic orbitals of the transition metal constituent and the 2s and 2p atomic orbitals of the boron atom. From these

atomic orbitals, 10 MOs may be constructed, as shown in Figure 11. The bonding orbitals here are of σ and π symmetry and are labeled as 1σ, 2σ, and 1π. The 1σ orbital is a bonding combination of the transition metal ndσ orbital and the 2s orbital of boron. This orbital was previously considered to be nonbonding,[9] but recent studies have concluded that it has significant bonding character, leading to the suggestion that RhB, for example, has a quadruple bond.[67, 68] The 2σ orbital is also a bonding orbital, and is primarily a combination of the metal ndσ and boron 2pσ atomic orbitals. The composition of these σ orbitals varies to some degree as one moves across the transition metal series. The 1π pair of orbitals are bonding combinations of the metal ndπ and boron 2pπ atomic orbitals.

Above these orbitals lie the essentially nonbonding 3σ MO, which in our calculations consists mostly of metal (n+1)s character. In contrast, however, a spectroscopic study of the hyperfine splitting in CoB shows that this orbital is roughly 55% metal (n+1)s in character.[69] The remaining character is suggested to be boron 2pσ, although this has not been directly determined because the boron hyperfine splitting was too small to measure.[69] Lying close to the 3σ MO is the nonbonding 1δ MO, which is of nearly pure transition metal ndδ character.

Finally, at much higher energies lie the strongly antibonding 2π and 4σ orbitals. These are the counterparts of the bonding 1π and 2σ orbitals, respectively. They remain empty in the ground states of all of the transition metal borides, and are irrelevant to any considerations of the chemical bonding in the ground states of these species.

While no previous experimental data on ScB, TiB, or VB exist, the neutral molecules and their singly ionized analogs have been studied systematically using multireference configuration interaction (MRCI) methods.[37, 47, 70-72] Černušák *et al.* calculated two possible candidates for the ground state of ScB: $1\sigma^2 2\sigma^2 1\pi^2$, $^3\Sigma^-$ and $1\sigma^2 2\sigma^1 3\sigma^1 1\pi^2$, $^5\Sigma^-$. Ultimately, a calculated 216 $cm^{-1}$

splitting between the two states gave rise to $^5\Sigma^-$ being the ground electronic state.[47] Tzeli *et al.* also employed MRCI methods to calculate electronic states of ScB, but included additional core correlation and scalar relativistic effects that increased the energy difference between the $X\,^5\Sigma^-$ and $a\,^3\Sigma^-$ states to 1100 $cm^{-1}$.[37] Both of these computational studies also report that the $X\,^5\Sigma^-$ electronic state adiabatically dissociates to Sc in its first excited state, $3d^24s^1$, $a\,^4F$, as is required by spin conservation. Černušák and Tzeli report bond dissociation energies of 3.304 eV and 3.25 eV to this excited separated atom limit, respectively. Both studies find that the bond dissociation energy for ScB is nearly halved when dissociation to the ground separated atom limit is considered, as is measured in our experiments. Černušák and Tzeli are in perfect agreement for this value: 1.787 eV and 1.79 eV, respectively. Both calculations for the BDE of ScB agree with our measured value of 1.72(6) eV.

Along with ScB, Tzeli *et al.* also calculated the ground state, low-lying excited states, and dissociation energies of TiB and VB.[37] Analogous to the dissociation channels of ScB, the calculated ground electronic states of TiB ($1\sigma^22\sigma^13\sigma^11\pi^21\delta^1$, $^6\Delta$) and VB ($1\sigma^22\sigma^13\sigma^11\pi^21\delta^2$, $^7\Sigma^+$) correlate to excited states of the metal atoms in which a 4s electron has been promoted to a 3d orbital, resulting in a high spin atomic state (Ti $3d^34s^1$, $a\,^5F$ and V $3d^44s^1$, $a^6D$). When corrected for dissociation to the ground separated atom limit, the BDEs of these species are 1.81 eV (TiB) and 2.01 eV (VB). These are about 0.15 eV less than our values of 1.956(16) eV (TiB) and 2.150(16) eV (VB).

The early 3d transition metal borides have also been systematically studied by Zhijian using density functional theory (DFT) with the B3LYP functional and the 6-311++G(3df) basis set.[73] This study calculated the BDEs of ScB, TiB, and VB to be 1.86 eV, 2.36 eV, and 2.13 eV, respectively. Although the BDE of TiB is overestimated by 0.4 eV compared to our result, the

values for ScB and VB are in reasonable agreement with our experimental measurements and the values calculated by Tzeli. It is also noteworthy that the ground electronic states reported in this DFT study are in agreement with the ground electronic states calculated by MRCI methods for ScB,[37, 47] TiB,[37] and VB.[37]

There exist in the literature commonly reported BDEs of ScB and TiB of 65 kcal $mol^{-1}$ (2.8 eV) and < 72 kcal $mol^{-1}$ (<3.1 eV),[43] which have been erroneously described as experimental measurements. These values have been derived using empirical correlations following a method due to Pauling.[74] The Pauling approach estimates the bond energy of a heterogeneous diatomic molecule as the geometric mean of the bond energies of the homoatomic counterparts, with an added ionic contribution based on the electronegativity difference of the atoms. The dissociation energies estimated by this method for ScB and TiB grossly overestimate the BDEs of the molecules. A complete summary of past studies on ScB, TiB, and VB is provided in Table 1.

### B. The 4d Early Transition Metal Borides: YB, ZrB, and NbB

No previous experimental work has been done on YB, ZrB, or NbB. A previous estimate of the BDE of YB obtained using the Pauling Method provides a value of 2.99 eV,[43] almost 1 eV greater than our measured value of 2.057(3) eV. Kharat *et al.* calculated ground state spin multiplicities and binding energies of the 4d MBs using DFT with the B3LYP functional and LANL2DZ basis set.[40] The calculation for YB returned a binding energy of 2.17 eV, 0.12 eV greater than our result, and predicted a quintet ground state. However, the B3LYP/LANL2DZ method grossly overestimated the BDE's of ZrB and NbB, providing values about 1.5 eV and 0.5 eV higher than our results of 2.573(5) eV and 2.989(12) eV, respectively. This calculation predicted ZrB and NbB to have sextet and triplet ground states, respectively.

Unfortunately, the study by Kharat *et al.* did not publish any of the ground state electronic configurations of the 4d MB's. Because comparing and contrasting the BDEs of MX molecules in the context of their electronic structure is helpful for building an understanding of the bonding in these species, DFT was employed in the current study to calculate ground state electronic symmetries and BDEs of the 4d transition metal borides. The B97-1 density functional was used with relativistic pseudopotentials and the correlation-consistent basis sets of the Stuttgart-Cologne group.[60, 63, 65, 66] More specific details on the computational methods employed are described in Section III.

Ultimately, these computations provided excellent agreement between the calculated and measured BDEs for the early 4d MBs. The differences between the calculated and measured values were all within 2 kcal $mol^{-1}$ for YB, ZrB, and NbB. For ground state calculations, we found the same ground state spin multiplicities for YB and ZrB as Kharat *et al.* reported but found that the ground state spin multiplicity for NbB is quintet, and not triplet as originally reported. The ground states of YB, ZrB, and NbB were computed to be $^5\Sigma^-$ ($1\sigma^2\ 2\sigma^1\ 3\sigma^1\ 1\pi^2$), $^6\Delta$ ($1\sigma^2\ 2\sigma^1\ 3\sigma^1\ 1\pi^2\ 1\delta^1$), and $^5\Pi/^5\Phi$ ($1\sigma^2\ 2\sigma^1\ 3\sigma^1\ 1\pi^3\ 1\delta^1$), respectively. In the case of NbB, the calculation uses real forms of the $1\pi$ and $1\delta$ orbitals, leading to a superposition of the $^5\Pi$ and $^5\Phi$ states. YB and ZrB have the same ground state as their isoelectronic 3d counterparts, ScB and TiB. Tabulated results from the DFT studies on YB, ZrB, and NbB, as well as their experimentally measured BDEs, are given in Table 2.

### C. The 5d Early Transition Metal Borides: LaB, HfB, TaB, and WB

LaB has been studied with *ab initio* Diffusion Monte Carlo (DMC) and DFT computational methods.[41, 46] In the *ab initio* DMC study, trial wavefunctions were generated using the B3LYP and B3PW91 functionals. Regardless of the trial wavefunction used, the $D_e$ of

LaB was grossly overestimated, 4.16 eV and 3.78 eV for the B3LYP and B3PW91 functionals, respectively,[46] in comparison to our measurement of 2.086(18) eV. Although $D_0$ for LaB was not explicitly reported in this *ab initio* DMC study, the $D_e$ value should be a fair estimation of the calculated bond dissociation energy in the context of these calculations. Kalamse *et al.* investigated LaB using DFT with the B3LYP functional and LANL2DZ basis set and reported a BDE of 2.49 eV,[41] which is much closer to our measurement. Although there is a large discrepancy for the BDE between these two studies, they both agree that the ground state spin multiplicity is quintet. The authors of the *ab initio* DMC study did not report an electronic symmetry for the ground state.[46] With B3LYP/LANL2DZ, the ground term of LaB is calculated to be $^5\Sigma^-$.[41] As with ScB, TiB, and YB, Gingerich used the Pauling method to estimate the BDE of LaB as 3.51 eV, nearly 1.5 eV greater than our measured value.[43]

Kalamse *et al.* also calculated binding energies and ground electronic states of HfB, TaB, and WB in their systematic study using B3LYP/LANL2DZ on the 5d monoborides.[41] The binding energies reported for HfB, TaB, and WB are 2.70 eV, 2.49 eV, and 2.74 eV, respectively. These are all within 0.21 eV of our results. As is the case for the early 3d and 4d transition metal borides, none of the early 5d MBs have been spectroscopically investigated, leaving their electronic ground states experimentally unconfirmed. The only ground states in the literature for HfB, TaB, and WB are from the calculations performed by Kalamse *et al.* who report ground states of $^4\Sigma^-$, $^3\Sigma^+$, and $^6\Sigma^-$, respectively.[41] However, the ground state configuration Kalamse *et al.* lists for WB, $1\sigma^2\ 2\sigma^1\ 3\sigma^1\ 1\pi^3\ 1\delta^2$, actually gives a $^6\Pi$ ground state. Moreover, the study also reports obviously incorrect ionization energies for HfB and IrB of -0.69 eV and 4.66 eV, respectively.[41] Further, Kalamse's predicted ground state of OsB, $^4\Delta$, also seems to be in error.[9] Because of these issues, we employed our own DFT calculations on LaB, HfB, TaB, and

WB for clarification purposes. See Section III for details on the computational methods used.

In our studies, HfB is calculated to have a $^4\Sigma^-$ ($1\sigma^2\ 2\sigma^1\ 3\sigma^2\ 1\pi^2$) ground state configuration and a BDE of 2.60 eV, in superb agreement with our measured value of 2.593(3) eV. The other group 4 borides, TiB and ZrB, are calculated to have a $^6\Delta$ ($1\sigma^2\ 2\sigma^1\ 3\sigma^1\ 1\pi^2\ 1\delta^1$) ground state. Instead, HfB is predicted to fill its nonbonding 3σ orbital before placing an unpaired electron in the nonbonding 1δ orbital.

Moving across the 5d transition metal period, we calculate TaB to have a $^5\Delta$ ($1\sigma^2\ 2\sigma^1\ 3\sigma^2\ 1\pi^2\ 1\delta^1$) ground state. However, a calculated low-lying $^3\Pi$ ($1\sigma^2\ 2\sigma^1\ 3\sigma^2\ 1\pi^3$) electronic state competes with the $^5\Delta$ state to be the true ground state of TaB and is found to have a vertical excitation energy of only 0.07 eV. Regardless of which of these is ultimately shown to be the ground state, TaB differs from VB and NbB by placing two electrons in the 6s-like 3σ orbital. We find that the $^3\Sigma^+$ electronic state that Kalamse calculated to be the ground state of TaB lies about 0.5 eV above the $^5\Delta$ ground state. Spectroscopic studies are needed to confirm the ground state of TaB and higher levels of theory can be used to establish the ordering of the low-lying $^5\Delta$, $^3\Pi$, and $^3\Sigma^+$ states. Our DFT result provides the BDE of TaB to be 2.96 eV, in fair agreement with our measured value of 2.700(3) eV.

We compute the ground electronic state of WB to be of $^6\Sigma^+$ ($1\sigma^2\ 2\sigma^1\ 3\sigma^2\ 1\pi^2\ 1\delta^2$) symmetry and the BDE to be about 0.16 eV higher in energy than our measured value. In our calculations, the $^6\Pi$ state that Kalamse obtains for the WB ground state lies vertically 0.2 eV higher in energy than the $^6\Sigma^+$ ground state, creating ambiguity about the ground state of WB at this level of theory. A spectroscopic investigation into the true ground state of WB is warranted. A summary of all of these findings on LaB, HfB, TaB, and WB can be found in Table 3.

Finally, it should be noted that these 5d transition metal borides are subject to strong spin-

orbit effects, which are neglected in all of these computational treatments. Computing the atomic spin-orbit stabilization as described in Ref. 14 leads to reductions in the computed BDEs of LaB, HfB, TaB, and WB of 0.08, 0.34, 0.44, and 0.55 eV, respectively, due to the lowering of the ground separated atom asymptote. Stabilization of the molecular ground state leads to an increase in the computed BDE by an amount that depends strongly on the molecular ground state and is estimated by first order perturbation theory, as described in Ref. 14, as 0.21 eV for the $^5\Delta$ state of TaB. The first order stabilization of the calculated ground states of LaB, HfB, and WB is zero, because these are all $\Sigma$ states with no first-order spin-orbit splitting. Because the spin-orbit stabilization of the molecular state is generally smaller than the stabilization at the ground separated atom limit, spin-orbit effects are generally expected to reduce the calculated BDE, sometimes significantly. Because of the uncertainty associated with the determination of the ground molecular state, coupled with our inability to calculate second- and higher-order spin-orbit effects, we have chosen not to apply these corrections to our computed BDEs. We simply note that a computational method that reproduces our measured BDEs, but fails to include spin-orbit corrections, may give good results due to a fortunate accident.

**D. Derived Quantities**

To our knowledge, ionization energies, cationic BDEs, and anionic BDEs have not been measured for any of the early transition metal borides. There exist experimental and theoretical studies on $VB^+$ and $VB_n^+$ clusters and their roles in methane activation, but no quantities relevant to Eqn. 1.1 are reported.[75-78] Likewise, electron spin resonance (ESR) spectroscopy was used to investigate $YB^+$ and assign an electronic ground state of $^4\Sigma^-$ for the molecule, but no thermochemical information was reported.[79] Because of this lack of information, Eqn. 1.1 cannot be employed to derive additional information on the early transition metal borides. However,

because the atomic enthalpy of formation at 0 K is known for the atomic constituents of these molecules, Eqn. 1.2 can be used with the BDEs to derive the molecular enthalpy of formation at 0 K. These values are provided in Table 4.

### E. Periodic Trends of the Early Transition Metal Borides

The measured BDEs and the computed properties of the early transition metal borides are summarized in Table 5. It is obvious that the 3d borides are less strongly bound that the corresponding 4d and 5d borides, which exhibit similar BDEs. More quantitatively, the early 4d and 5d metal borides are bound approximately 25% more strongly than their 3d counterparts. This trend mimics what is observed for the late transition metal borides (see Table 6), where the bond energies of the 4d and 5d borides are greatly enhanced.[9] It has also been observed in the transition metal carbides,[5, 15] silicides,[5, 16, 17] sulfides,[19, 20] and selenides[22, 23] that the 3d series gives much weaker bonds than are found in the congeners from the subsequent periods. This observation may be rationalized by the fact that the 3d orbitals are much smaller than the 4d and 5d orbitals, and the ratio $\langle r \rangle_{nd} / \langle r \rangle_{(n+1)s}$ is much smaller for the 3d orbitals than the 4d and 5d orbitals as well.[80] In a sense, the 3d orbitals are buried under the 4s orbital, causing the 3d series to form weaker bonds than the 4d and 5d series quite generally.

Table 5 also shows that the 3d and 4d early transition metal borides only place one electron in the 3σ orbital, which is primarily 4s or 5s in character. This trend is followed in the late 3d borides as well, suggesting that when an electron is removed from the 4s orbital, it allows the boron atom to approach sufficiently to form a σ bond to the underlying 3dσ orbital.[37] The resulting dσ-pσ bond is much stronger than that formed to the 4s orbital, allowing the molecule to recoup the promotion energy associated with the promotion of an (n+1)s electron to the nd

orbital. In the late 4d borides, RhB and RuB,[81-84] the 3σ orbital is empty, allowing even more effective bonding to the 4d orbitals without interference from an occupied 5s orbital.

In the 5d series, Table 5 shows that with the exception of LaB, the 6s-like 3σ orbital remains doubly occupied in the early transition metal borides. This fact undoubtedly results from the relativistic stabilization of the 6s orbital, which favors occupation of the 3σ orbital. The relativistic contraction of the 6s orbital also leads to an increase in the orbital size ratio, $\langle r \rangle_{nd} / \langle r \rangle_{(n+1)s}$, which leads to more favorable bonding with the 5d orbitals.[80] Lanthanum boride is the exception here, but it must be remembered that La (Z=57) is not the predecessor to Hf (Z=72) in the periodic table, Lu (Z=71) is. Because relativistic effects scale so strongly with atomic number, the relativistic stabilization of the 6s orbital in La is only 5.4% of the 6s orbital energy.[80] In Lu, Hf, and Ta the stabilization is 11.9, 13.9, and 15.6%, respectively.[80] Thus, relativistic effects in LaB are much less important than in the remaining 5d borides, allowing the 6s-like 3σ orbital to remain singly-occupied in LaB.

Within one period, the bond dissociation energy increases as one moves from group 3 to group 4 to group 5 (and on to group 6 in the case of WB). In the 3d and 4d periods, the additional electrons are generally added to nonbonding 1δ orbitals, making it difficult to understand why the bond energy should increase. Part of the explanation in these periods, however, results from the fact that all of the ground states of these molecules correlate to high spin $(n+1)s^1\ nd^n$ states of the atoms, and the promotion energy required to reach this state decreases as one moves across the 3d or 4d period. In a sense, the later molecules in each series do not have to waste as much energy in preparing the metal atom to bond, and are able to achieve larger BDEs as a result. In the case of NbB, the last electron is placed the bonding 1π orbital, leading to the only $1\pi^3$ configuration among this set of molecules. The development of a π bond

order of 1.5 undoubtedly contributes to the fact that NbB has the strongest bond among the species reported here.

Aluminum and boron both have the same electron deficient valence configuration of $ns^2\ np^1$, allowing for comparisons of the early transition metal-aluminum and transition metal-boron bonds. Every transition metal aluminide, AlM, has been systematically studied with density functional theory.[85, 86] In all cases except AlAg, the BDE of the transition metal boride is much stronger than the calculated BDE of its analogous AlM species. Among the early transition metal aluminides, jet-cooled AlV and AlY have also been investigated using R2PI spectroscopy.[11, 87] For AlV, the observation of spectroscopic transitions originating from both $\Omega''=0$ and $\Omega''=1$ led to the suggestion that the ground state was either $1\sigma^2\ 2\sigma^2\ 3\sigma^1\ 1\pi^2\ 1\delta^1$, $^5\Delta$ or $1\sigma^2\ 2\sigma^2\ 1\pi^2\ 1\delta^2$, $^5\Sigma^+$;[11] the former is the ground state in the DFT calculation.[85, 86] This differs from the $1\sigma^2\ 2\sigma^1\ 3\sigma^1\ 1\pi^2\ 1\delta^2$, $^7\Sigma^+$ ground state obtained for VB. For AlY, the ground state was found to have $\Omega''=0$ and on the basis of a comparison to the $AlY^+$ ESR spectrum[79] it was concluded that the AlY ground state is $^3\Sigma^-$ ($1\sigma^2\ 2\sigma^2\ 1\pi^2$),[87] as was confirmed in the same DFT study.[85] Again, this differs from the YB $1\sigma^2\ 2\sigma^1\ 3\sigma^1\ 1\pi^2$, $^5\Sigma^-$ ground state. A comparison of the DFT calculations on the early transition metal borides to the corresponding aluminides shows that in the aluminides, the $2\sigma^1\ 3\sigma^1$ set of unpaired electrons (as found in ScB, TiB, VB, and YB) are instead paired in a single σ orbital. Another distinction that may be made between the aluminides and the borides is that in the borides, the σ-bond is usually formed by the interaction of the boron 2pσ and the transition metal ndσ orbitals.[37] In contrast, the late 3d transition metal aluminides form a σ-bond through the Al 3pσ – M 4sσ interaction.[86] In the early transition metal aluminides, the metal atom undergoes sdσ hybridization prior to the formation of a σ-bond to the 3pσ orbital of aluminum.[86]

The most obvious bonding trend of the transition metal borides is the general increase in BDEs as the period is traversed, displayed in Figure 12. This results from the fact that as one moves across the series, electrons are sequentially added to either bonding orbitals or nominally nonbonding orbitals, with the antibonding orbitals remaining empty across the entire series. A few anomalies are found, however. First, there is a striking drop in BDE for CrB and MnB, and again for CuB in the 3d period. In these species, the σ-bond is formed via a $4s_{\sigma M}$-$2p_{\sigma B}$ bonding interaction, rather than the $3d_{\sigma M}$-$2p_{\sigma B}$ bonding that is present in all of the other 3d borides.[37] For CrB and MnB this is probably due to the disruption of exchange energy that would occur if the half-filled $3d^5$ subshell were broken. In CuB, the 3d orbitals have dropped so low in energy that they are now core-like and are unable to engage very significantly in the bonding. Second, there is an unexpectedly large increase in the BDE in moving from MoB to TcB. Our DFT calculations predict that TcB forms two full π-bonds as compared to the π bond order of 1.5 in MoB. Because of the increased accessibility of the 4d orbitals compared to the 3d orbitals, this leads to a significant increase in BDE. The other anomaly in the 4d series is the large drop in BDE when PdB and AgB are reached. The low BDE of palladium diatomics has also been seen in the bonding trends of PdN, PdC, PdSi, and PdO.[15, 17, 40, 88] The anomalous $4d^{10}$ $5s^0$ ground configuration of Pd demonstrates that the 4d orbitals in palladium have also become nearly core-like, greatly weakening the bonding in all diatomic compounds of palladium. The continued dropping of the nd orbitals into the core further weakens the bond in the coinage metal borides, as also occurs in other coinage metal p-block diatomics.[89-91]

## 6. CONCLUSIONS

The bond dissociation energies of 10 diatomic early transition metal borides (M = Sc, Ti, V, Y, Zr, Nb, La, Hf, Ta, W) have been measured by the observation of a predissociation threshold using R2PI spectroscopy. This marks the first time that the BDEs of these species have been experimentally reported. With this work, 10 additional highly precise thermochemical values are now available for use in benchmarking quantum chemical computations. Of equal importance, a quantitative understanding of the transition metal-boron bond emerges from these BDE values and the previously reported BDEs of the late transition metal boride molecules. Generally, the bond strengths of the transition metal borides increase as one traverses the period from left to right, or as one goes down a column. Anomalies exist, however, that are a testament to the variety of bonding schemes that the MB molecules can exhibit. Mainly, these bonding schemes are different iterations of how the bonding σ and π orbitals are filled and whether the σ bond is formed to the ndσ orbital or to the (n+1)s orbital of the metal. Diatomic transition metal borides can display one-and-a-half, double, triple, and even quadruple bonds, with the latter being recently discovered in RhB.[67]Within the early transition metal borides of the 3d and 4d series, the ground state tends to arise from the high-spin coupling of the $(n+1)s^1\ nd^n$ configuration of the metal atom with the ground $2p^1$ configuration of boron, a result that is only possible due to the electron-deficient nature of both atoms. For most of the early borides of the 5d series, however, the ground state arises from the $6s^2\ 5d^n$ configuration of the atom.
In contrast to the high spin multiplicities of the early transition metal borides, the late transition metal borides have low spin multiplicities and are all thought to be at least triply bonded. Future work from this group on BDE measurements for boron containing systems will focus on the lanthanide borides and the early transition metal and lanthanide diborides, $MB_2$ and $LnB_2$.

## AUTHOR INFORMATION


### Corresponding Author

*E-mail: morse@chem.utah.edu . Fax: (801)-581-8433

ORCID

Michael D. Morse: 0000-0002-2386-7315


Notes

The authors declare no competing financial interest.

## ACKNOWLEDGMENT


The authors thank the National Science Foundation for support of this research under Grant No. CHE-1952924. Christopher Nielson would also like to thank the Undergraduate Research Opportunities Program at the University of Utah for financial support. The authors also thank Samantha K. Walker for her extended technical troubleshooting of the calculations performed in this work. We also thank the Center for High Performance Computing at the University of Utah for their technical resources and support.

**REFERENCES:**


(1) James, A. M.; Kowalczyk, P.; Langlois, E.; Campbell, M. D.; Ogawa, A.; Simard, B. Resonant Two Photon Ionization Spectroscopy of the Molecules $V_2$, VNb, $Nb_2$. *J. Chem. Phys.* **1994**, *101*, 4485-4495.

(2) Yang, D. S.; James, A. M.; Rayner, D. M.; Hackett, P. A. Pulsed Field Ionization Zero Kinetic Energy Photoelectron Spectroscopy of the Vanadium Dimer Molecule. *J. Chem. Phys.* **1995**, *102*, 3129-3134.

(3) Spain, E. M.; Morse, M. D. Bond Strengths of Transition Metal Dimers: TiV, $V_2$, TiCo, and VNi. *J. Phys. Chem.* **1992**, *96*, 2479-2486.

(4) Russon, L. M.; Heidecke, S. A.; Birke, M. K.; Conceicao, J.; Morse, M. D.; Armentrout, P. B. Photodissociation Measurements of Bond Dissociation Energies: $Ti_2^+$, $V_2^+$, $Co_2^+$, and $Co_3^+$. *J. Chem. Phys.* **1994**, *100*, 4747-4755.

(5) Sevy, A.; Merriles, D. M.; Wentz, R. S.; Morse, M. D. Bond Dissociation Energies of ScSi, YSi, LaSi, ScC, YC, LaC, CoC, and YCH. *J. Chem. Phys.* **2019**, *151*, 024302.

(6) Garton, W. R. S.; Wilson, M. Auto-Ionization Rydberg Series in the Spectrum of La I. *Astrophys. J.* **1966**, *145*, 333-336.

(7) Kramida, A.; Ralchenko, Y.; Reader, J.; and NIST ASD Team, *NIST Atomic Spectra Database (version 5.8)*; National Institute of Standards and Technology, Gaithersburg, MD, 2020.

(8) Kickel, B. L.; Armentrout, P. B. Guided Ion Beam Studies of the Reactions of Group 3 Metal Ions ($Sc^+$, $Y^+$, $La^+$, and $Lu^+$) with Silane. Electronic State Effects, Comparison to Reactions with Methane, and $M^+$-$SiH_x$ (x = 0-3) Bond Energies. *J. Am. Chem. Soc.* **1995**, *117*, 4057-4070.

(9) Merriles, D. M.; Tieu, E.; Morse, M. D. Bond Dissociation Energies of FeB, CoB, NiB, RuB, RhB, OsB, IrB, and PtB. *J. Chem. Phys.* **2019**, *151*, 044302.

(10) Behm, J. M.; Arrington, C. A.; Morse, M. D. Spectroscopic Studies of Jet-Cooled AlNi. *J. Chem. Phys.* **1993**, *99*, 6409-6415.

(11) Behm, J. M.; Brugh, D. J.; Morse, M. D. Spectroscopic Analysis of the Open 3d Subshell Transition Metal Aluminides: AlV, AlCr, and AlCo. *J. Chem. Phys.* **1994**, *101*, 6487-6499.

(12) Johnson, E. L.; Davis, Q. C.; Morse, M. D. Predissociation Measurements of Bond Dissociation Energies: VC, VN, and VS. *J. Chem. Phys.* **2016**, *144*, 234306.

(13) Matthew, D. J.; Tieu, E.; Morse, M. D. Determination of the Bond Dissociation Energies of FeX and NiX (X = C, S, Se). *J. Chem. Phys.* **2017**, *146*, 144310.

(14) Sevy, A.; Huffaker, R. F.; Morse, M. D. Bond Dissociation Energies of Tungsten Molecules: WC, WSi, WS, WSe, and WCl. *J. Phys. Chem. A* **2017**, *121*, 9446-9457.

(15) Sevy, A.; Matthew, D. J.; Morse, M. D. Bond Dissociation Energies of TiC, ZrC, HfC, ThC, NbC, and TaC. *J. Chem. Phys.* **2018**, *149*, 044306.

(16) Sevy, A.; Sorensen, J. J.; Persinger, T. D.; Franchina, J. A.; Johnson, E. L.; Morse, M. D. Bond Dissociation Energies of Diatomic Transition Metal Silicides: TiSi, ZrSi, HfSi, VSi, NbSi, and TaSi. *J. Chem. Phys.* **2017**, *147*, 084301.

(17) Sevy, A.; Tieu, E.; Morse, M. D. Bond Dissociation Energies of FeSi, RuSi, OsSi, CoSi, RhSi, IrSi, NiSi, and PtSi. *J. Chem. Phys.* **2018**, *149*, 174307.

(18) Sorensen, J. J.; Tieu, E.; Sevy, A.; Merriles, D. M.; Nielson, C.; Ewigleben, J. C.; Morse, M. D. Bond Dissociation Energies of Transition Metal Oxides: CrO, MoO, RuO, and RhO. *J. Chem. Phys.* **2020**, *153*, 074303.

(19) Sorensen, J. J.; Tieu, E.; Morse, M. D. Bond Dissociation Energies of the Diatomic Late Transition Metal Sulfides: RuS, OsS, CoS, RhS, IrS, and PtS. *J. Chem. Phys.* **2020**, *152*, 244305.

(20) Sorensen, J. J.; Tieu, E.; Nielson, C.; Sevy, A.; Tomchak, K. H.; Morse, M. D. Bond Dissociation Energies of Diatomic Transition Metal Sulfides: ScS, YS, TiS, ZrS, HfS, NbS, and TaS. *J. Chem. Phys.* **2020**, *152*, 194307.

(21) Sorensen, J. J.; Tieu, E.; Morse, M. D. Bond Dissociation Energies of Lanthanide Sulfides and Selenides. *J. Chem. Phys.* **2021**, *154*, 124307.

(22) Sorensen, J. J.; Persinger, T. D.; Sevy, A.; Franchina, J. A.; Johnson, E. L.; Morse, M. D. Bond Dissociation Energies of Diatomic Transition Metal Selenides: TiSe, ZrSe, HfSe, VSe, NbSe, and TaSe. *J. Chem. Phys.* **2016**, *145*, 214308.

(23) Sorensen, J. J.; Tieu, E.; Morse, M. D. Bond Dissociation Energies of Diatomic Transition Metal Selenides: ScSe, YSe, RuSe, OsSe, CoSe, RhSe, IrSe, and PtSe. *J. Chem. Phys.* **2020**, *152*, 124305.

(24) Nagamatsu, J.; Nakagawa, N.; Muranaka, T.; Zenitani, Y.; Akimitsu, J. Superconductivity at 39 K in Magnesium Diboride. *Nature* **2001**, *410*, 63.

(25) Gou, H.; Dubrovinskaia, N.; Bykova, E.; Tsirlin, A. A.; Kasinathan, D.; Schnelle, W.; Richter, A.; Merlini, M.; Hanfland, M.; Abakumov, A. M.et al. Discovery of a Superhard Iron Tetraboride Superconductor. *Phys. Rev. Lett.* **2013**, *111*, 157002.

(26) Carnicom, E. M.; Xie, W.; Klimczuk, T.; Lin, J.; Górnicka, K.; Sobczak, Z.; Ong, N. P.; Cava, R. J. $TaRh_2B_2$ and $NbRh_2B_2$: Superconductors with a Chiral Noncentrosymmetric Crystal Structure. *Sci. Adv.* **2018**, *4*, eaar7969.

(27) Mayrhofer, P. H.; Mitterer, C.; Wen, J. G.; Greene, J. E.; Petrov, I. Self-Organized Nanocolumnar Structure in Superhard $TiB_2$ Thin Films. *Appl. Phys. Lett.* **2005**, *86*, 131909.

(28) Chung, H.-Y.; Weinberger, M. B.; Levine, J. B.; Kavner, A.; Yang, J.-M.; Tolbert, S. H.; Kaner, R. B. Synthesis of Ultra-Incompressible Superhard Rhenium Diboride at Ambient Pressure. *Science* **2007**, *316*, 436-439.

(29) Raju, G. B.; Basu, B.; Suri, A. K. Thermal and Electrical Properties of $TiB_2$–$MoSi_2$. *Int. J. Refract. Met. and Hard Mat.* **2010**, *28*, 174-179.

(30) Passerone, A.; Valenza, F.; Muolo, M. L. A Review of Transition Metals Diborides: from Wettability Studies to Joining. *J. Mater. Sci.* **2012**, *47*, 8275-8289.

(31) Moraes, V.; Riedl, H.; Fuger, C.; Polcik, P.; Bolvardi, H.; Holec, D.; Mayrhofer, P. H. Ab initio Inspired Design of Ternary Boride Thin Films. *Sci. Rep.* **2018**, *8*, 9288.

(32) Yuan, H.; Li, Z.; Yang, J. Transition-Metal Diboride: A New Family of Two-Dimensional Materials Designed for Selective $CO_2$ Electroreduction. *J. Phys. Chem. C* **2019**, *123*, 16294-16299.

(33) Qin, G.; Cui, Q.; Du, A.; Wang, W.; Sun, Q. Transition Metal Diborides: A New Type of High-performance Electrocatalysts for Nitrogen Reduction. *ChemCatChem* **2019**, *11*, 2624-2633.

(34) Wang, N.; Fu, Z.; Legut, D.; Wei, B.; Germann, T. C.; Zhang, R. Designing Ultrastrong 5d Transition Metal Diborides with Excellent Stability for Harsh Service Environments. *Phys. Chem. Chem. Phys.* **2019**, *21*, 16095-16107.

(35) Fehlner, T. P. Molecular Models of Solid State Metal Boride Structures. *J. Solid State Chem.* **2000**, *154*, 110-113.

(36) Sergeeva, A. P.; Popov, I. A.; Piazza, Z. A.; Li, W.-L.; Romanescu, C.; Wang, L.-S.; Boldyrev, A. I. Understanding Boron through Size-Selected Clusters: Structure, Chemical Bonding, and Fluxionality. *Acc. Chem. Res.* **2014**, *47*, 1349-1358.

(37) Tzeli, D.; Mavridis, A. Electronic Structure and Bonding of the 3d Transition Metal Borides, MB, M = Sc, Ti, V, Cr, Mn, Fe, Co, Ni, and Cu through All Electron *ab initio* Calculations. *J. Chem. Phys.* **2008**, *128*, 034309.

(38) Borin, A. C.; Gobbo, J. P. Electronic Structure of the Ground and Low-Lying Electronic States of MoB and $MoB^+$. *Int. J. Quantum Chem.* **2011**, *111*, 3362-3370.

(39) Borin, A. C.; Gobbo, J. P.; Castro, C. A. M. The Low-Lying Electronic States of ReB. *J. Mol. Model.* **2014**, *20*, 1-5.

(40) Kharat, B.; Deshmukh, S. B.; Chaudhari, A. 4d Transition Metal Monoxides, Monocarbides, Monoborides, Mononitrides, and Monofluorides: A Quantum Chemical Study. *Int. J. Quantum Chem.* **2009**, *109*, 1103-1115.

(41) Kalamse, V.; Gaikwad, S.; Chaudhari, A. Computational Study of 5d Transition Metal Mononitrides and Monoborides Using Density Functional Method. *Bull. Mater. Sci.* **2010**, *33*, 233-238.

(42) Harrison, J. F. Electronic Structure of Diatomic Molecules Composed of a First-Row Transition Metal and Main-Group Element (H-F). *Chem. Rev.* **2000**, *100*, 679-716.

(43) Gingerich, K. A. Gaseous Metal Borides. I. Dissociation Energy of the Molecules ThB, ThP, and $Th_2$, and Predicted Dissociation Energies of Selected Diatomic Transition-Metal Borides. *High Temp. Sci.* **1969**, *1*, 258-267.

(44) Pople, J. A. Nobel Lecture: Quantum Chemical Models. *Rev. Mod. Phys.* **1999**, *71*, 1267-1274.

(45) DeYonker, N. J.; Peterson, K. A.; Steyl, G.; Wilson, A. K.; Cundari, T. R. Quantitative Computational Thermochemistry of Transition Metal Species. *J. Phys. Chem. A* **2007**, *111*, 11269-11277.

(46) Elkahwagy, N.; Ismail, A.; Maize, S. M. A.; Mahmoud, K. R. Diffusion Monte Carlo Calculations on LaB Molecule. *Chin. Phys. B* **2018**, *27*, 093102.

(47) Černušák, I.; Dallos, M.; Lischka, H.; Müller, T.; Uhlár, M. On the Ground and Some Low-Lying Excited States of ScB: A Multiconfigurational Study. *J. Chem. Phys.* **2007**, *126*, 214311.

(48) Hotop, H.; Lineberger, W. C. Binding Energies in Atomic Negative Ions: II. *J. Phys. Chem. Ref. Data* **1985**, *14*, 731-750.

(49) Reid, C. J. Electron Affinities of BH, $B_2$, BC and BN Molecules Determined Using Charge Inversion Spectrometry. *Int. J. Mass Spectrom. Ion Proc.* **1993**, *127*, 147-160.

(50) Glezakou, V.-A.; Taylor, P. R. On the Electron Affinity of $B_2$. *Eur. J. Mass Spectrom.* **2009**, *15*, 337-341.

(51) Gingerich, K. A. Gaseous Metal Borides. II. Mass-Spectrometric Evidence for the Molecules $UB_2$, UB, and CeB and Predicted Stability of Gaseous Diborides of Electropositive Transition Metals. *J. Chem. Phys.* **1970**, *53*, 746-748.

(52) Lindholm, N. F.; Brugh, D. J.; Rothschopf, G. K.; Sickafoose, S. M.; Morse, M. D. Optical Spectroscopy of Jet-Cooled NiSi. *J. Chem. Phys.* **2003**, *118*, 2190-2196.

(53) Stangassinger, A.; Knight, A. M.; Duncan, M. A. Photoionization Spectroscopy of NaAg. *Chem. Phys. Lett.* **1997**, *266*, 189-194.

(54) Johnson, E. L.; Morse, M. D. Resonant Two-Photon Ionization Spectroscopy of Jet-Cooled OsSi. *J. Chem. Phys.* **2015**, *143*, 104303.

(55) Matthew, D. J.; Morse, M. D. Resonant Two-Photon Ionization Spectroscopy of Jet-Cooled UN: Determination of the Ground State. *J. Chem. Phys.* **2013**, *138*, 184303.

(56) Wiley, W. C.; McLaren, I. H. Time-of-Flight Mass Spectrometer with Improved Resolution. *Rev. Sci. Instrum.* **1955**, *26*, 1150 - 1157.

(57) Frisch, M. J.; Trucks, G. W.; Schlegel, H. B.; Scuseria, G. E.; Robb, M. A.; Cheeseman, J. R.; Scalmani, G.; Barone, V.; Petersson, G. A.; Nakatsuji, H.et al. *Gaussian 16*, Rev. B.01; Gaussian, Inc.: Wallingford, CT, 2016.

(58) Hamprecht, F. A.; Cohen, A. J.; Tozer, D. J.; Handy, N. C. Development and Assessment of New Exchange-Correlation Functionals. *J. Chem. Phys.* **1998**, *109*, 6264-6271.

(59) Shee, J.; Rudshteyn, B.; Arthur, E. J.; Zhang, S.; Reichman, D. R.; Friesner, R. A. On Achieving High Accuracy in Quantum Chemical Calculations of 3d Transition Metal-Containing Systems: A Comparison of Auxiliary-Field Quantum Monte Carlo with Coupled Cluster, Density Functional Theory, and Experiment for Diatomic Molecules. *J. Chem. Theory Comput.* **2019**, *15*, 2346-2358.

(60) Peterson, K. A.; Figgen, D.; Dolg, M.; Stoll, H. Energy-Consistent Relativistic Pseudopotentials and Correlation Consistent Basis Sets for the 4d Elements Y-Pd. *J. Chem. Phys.* **2007**, *126*, 124101.

(61) Weigand, A.; Cao, X.; Yang, J.; Dolg, M. Quasirelativistic f-in-core Pseudopotentials and Core-Polarization Potentials for Trivalent Actinides and Lanthanides: Molecular Test for Trifluorides. *Theor. Chem. Acc.* **2010**, *126*, 117-127.

(62) Yang, J.; Dolg, M. Valence Basis Sets for Lanthanide 4f-in-core Pseudopotentials Adapted for Crystal Orbital *ab initio* Calculations. *Theor. Chem. Acc.* **2005**, *113*, 212-224.

(63) Dolg, M.; Stoll, H.; Preuss, H. Energy-Adjusted *ab initio* Pseudopotentials for the Rare Earth Elements. *J. Chem. Phys.* **1989**, *90*, 1730-1734.

(64) Dunning, T. H., Jr. Gaussian Basis Sets for Use in Correlated Molecular Calculations. I. The Atoms Boron through Neon and Hydrogen. *J. Chem. Phys.* **1989**, *90*, 1007-1023.

(65) Dolg, M.; Stoll, H.; Preuss, H. A Combination of Quasirelativistic Pseudopotential and Ligand Field Calculations for Lanthanoid Compounds. *Theor. Chim. Acta* **1993**, *85*, 441-450.

(66) Figgen, D.; Peterson, K. A.; Dolg, M.; Stoll, H. Energy-Consistent Pseudopotentials and Correlation Consistent Basis Sets for the 5d Elements Hf-Pt. *J. Chem. Phys.* **2009**, *130*, 164108.

(67) Cheung, L. F.; Chen, T.-T.; Kocheril, G. S.; Chen, W.-J.; Czekner, J.; Wang, L.-S. Observation of Four-Fold Boron-Metal Bonds in RhB($BO^-$) and RhB. *J. Phys. Chem. Lett.* **2020**, *11*, 659-663.

(68) Tzeli, D.; Karapetsas, I. Quadruple Bonding in the Ground and Low-Lying Excited States of the Diatomic Molecules TcN, RuC, RhB, and PdBe. *J. Phys. Chem. A* **2020**, *124*, 6667-6681.

(69) Dore, J. M.; Adam, A. G.; Tokaryk, D. W.; Linton, C. Hyperfine Analysis of the (2, 0) [18.3]3-$X^3\Delta_3$ Transition of Cobalt Monoboride. *J. Mol. Spectrosc.* **2019**, *360*, 44-48.

(70) Kalemos, A.; Mavridis, A. On the Electronic Structure of $ScB^+$: Ground and Low-Lying Excited States. *Adv. Quantum Chem.* **1998**, *32*, 69-91.

(71) Kalemos, A.; Mavridis, A. Bonding Investigation of the Ground and Low-Lying States of the Titanium Boride Cation, $TiB^+$. *J. Phys. Chem. A* **1998**, *102*, 5982-5992.

(72) Kalemos, A.; Mavridis, A. Ground and Low-Lying States of the Vanadium Boride Cation, $VB^+$: An ab Initio Investigation. *J. Phys. Chem. A* **1999**, *103*, 3336-3345.

(73) Zhijian, W. Density Functional Study of 3d-Metal Monoborides. *J. Mol. Struct.: THEOCHEM* **2005**, *728*, 167-172.

(74) Pauling, L. C. *The Nature of the Chemical Bond and the Structure of Molecules and Crystals. An Introduction to Modern Structural Chemistry. 3rd ed*; Cornell University Press: Ithaca, NY, 1960.

(75) Chen, Q.; Zhao, Y.-X.; Jiang, L.-X.; Li, H.-F.; Chen, J.-J.; Zhang, T.; Liu, Q.-Y.; He, S.-G. Thermal Activation of Methane by Vanadium Boride Cluster Cations $VB_n^+$ (n = 3–6). *Phys. Chem. Chem. Phys.* **2018**, *20*, 4641-4645.

(76) Chen, Q.; Jiang, L.-X.; Li, H.-F.; Chen, J.-J.; Zhao, Y.-X.; He, S.-G. Thermal Activation of Methane by Diatomic Vanadium Boride Cations. *Acta Phys. -Chim. Sin.* **2019**, *35*, 1014-1020.

(77) Tran, V. T.; Tran, Q. T. Geometric and Electronic Structures of $VB_4^{0/+}$ Clusters and Reactivity of the Cationic Cluster with Methane from Quantum Chemical Calculations. *J. Phys. Chem. A* **2019**, *123*, 9223-9233.

(78) Tran, T. H.; Tran, Q. T.; Tran, V. T. Mechanism of the Reaction of $VB_5^+$ Cluster with Methane from Density Functional Theory Calculations. *Comp. Theor. Chem.* **2020**, *1173*, 112701.

(79) Knight, L. B., Jr.; Babb, R. M.; King, G. M.; McKinley, A. J.; Morse, M. D.; Arrington, C. A. Laser Vaporization Generation of $Y^{10}B^+$, $Y^{11}B^+$, and $YAl^+$ for Electron Spin Resonance Studies in Neon Matrices at 4K: Comparison with Theoretical Calculations. *J. Chem. Phys.* **1993**, *98*, 4404-4412.

(80) Desclaux, J. P. Relativistic Dirac-Fock Expectation Values for Atoms with Z=1 to 120. *At. Data Nucl. Data Tables* **1973**, *12*, 311.

(81) Chowdhury, P. K.; Balfour, W. J. A Spectroscopic Study of the Rhodium Monoboride Molecule. *Mol. Phys.* **2007**, *105*, 1619-1624.

(82) Chowdhury, P. K.; Balfour, W. J. A Spectroscopic Characterization of the Electronic Ground State of Rhodium Monoboride. *J. Chem. Phys.* **2006**, *124*, 216101.

(83) Wang, N.; Ng, Y. W.; Cheung, A. S. C. Laser Induced Fluorescence Spectroscopy of RuB. *Chem. Phys. Lett.* **2012**, *547*, 21-23.

(84) Dore, J. M.; Adam, A. G.; Linton, C.; Tokaryk, D. W. High-Resolution Spectroscopy of the [18.4]2.5 - $X^2\Delta_{5/2}$ Transition of Ruthenium Monoboride (RuB). *J. Mol. Spectrosc.* **2020**, *372*, 111321.

(85) Ouyang, Y.; Wang, J.; Hou, Y.; Zhong, X.; Du, Y.; Feng, Y. First Principle Study of AlX (X=3d,4d,5d elements and Lu) Dimer. *J. Chem. Phys.* **2008**, *128*, 074305.

(86) Ouyang, Y.; Wang, J.; Liu, F.; Liu, Y.; Du, Y.; He, Y.; Feng, Y. Density Functional Study of 3d-Transition Metal Aluminides. *J. Mol. Struct. THEOCHEM* **2009**, *905*, 106-112.

(87) Arrington, C. A.; Langenberg, J. D.; Pinegar, J. C.; Morse, M. D.; Doverstål, M.; Sassenberg, U. Spectroscopy of Jet-Cooled AlY. *J. Phys. Chem.* **1995**, *99*, 2589-2593.

(88) Kretzschmar, I.; Schröder, D.; Schwarz, H.; Armentrout, P. B. The Binding in Neutral and Cationic 3d and 4d Transition-Metal Monoxides and -Sulfides. *Adv. Met. Semicond. Clusters* **2001**, *5*, 347-395.

(89) Li, Z.; Zhang, J.; Meng, D.; Yu, Y. Electronic Structure and Bonding Characters of the Two Lowest States of Copper, Silver, and Gold Monocarbides. *Comput. Theor. Chem.* **2011**, *966*, 97-104.

(90) Riekert, G.; Lamparter, P.; Steeb, S. Mass-Spectrometric Determination of the Dissociation Energy of the Gaseous Molecules Copper-Silicon (CuSi) and Silver-Silicon (AgSi). *Z. Metallkd.* **1981**, *72*, 765-768.

(91) Vander Auwera-Mahieu, A.; Peeters, R.; McIntyre, N. S.; Drowart, J. Mass Spectrometric Determination of Dissociation Energies of the Borides and Silicides of some Transition Metals. *Trans. Faraday Soc.* **1970**, *66*, 809-816.

(92) Hultgren, R.; Desai, P. D.; Hawkins, D. T.; Gleiser, M.; Kelley, K. K.; Wagman, D. D. *Selected Values of the Thermodynamic Properties of the Elements*; American Society for Metals: Metals Park, Ohio, 1973.

(93) Chase, M. W., Jr. *NIST-JANAF Thermochemical Tables, Fourth Edition*; American Institute of Physics for the National Institute of Standards and Technology: Washington, D.C., 1998.

(94) Goudreau, E. S.; Adam, A. G.; Tokaryk, D. W.; Linton, C. High Resolution Laser Spectroscopy of the [20.6]0.5-$X^2\Sigma^+$ Transition of Nickel Monoboride, NiB. *J. Mol. Spectrosc.* **2015**, *314*, 13-18.

(95) Ng, Y. W.; Pang, H. F.; Qian, Y.; Cheung, A. S. C. Electronic Transition of PdB. *J. Phys. Chem. A* **2012**, *116*, 11568-11572.

(96) Barysz, M.; Urban, M. Molecular Properties of Boron-Coinage Metal Dimers: BCu, BAg, BAu. In *Adv. Quantum Chem.*; Löwdin, P.-O., Sabin, J. R., Zerner, M. C., Karwowski, J., Karelson, M., Eds.; Academic Press, 1997; Vol. 28; pp 257-272.

(97) Pang, H. F.; Ng, Y. W.; Xia, Y.; Cheung, A. S. C. Electronic Transitions of IrB. *Chem. Phys. Lett.* **2011**, *501*, 257-262.

(98) Ng, Y. W.; Wong, Y. S.; Pang, H. F.; Cheung, A. S. C. Electronic Transitions of PtB. *J. Chem. Phys.* **2012**, *137*, 124302.

(99) Gingerich, K. A. Gaseous Metal Borides. III. Dissociation Energy and Heat of Formation of Gold Monoboride. *J. Chem. Phys.* **1971**, *54*, 2646-2650.

Table 1. Previous studies of ScB, TiB, and VB. [a]

| Molecule | Ground Term | $D_0$ (eV) | Methods | Authors | Year | Reference |
|---|---|---|---|---|---|---|
| ScB | | **1.72(6)** | Predissociation Threshold | | 2021 | This work |
| | $^5\Sigma^-$ | 1.79 | MRCI+Q | Tzeli and Mavridis | 2008 | 37 |
| | $^5\Sigma^-$ | 1.787 | MRCI+Q | Černušák *et al.* | 2007 | 47 |
| | $^5\Sigma^-$ | 1.86 | B3LYP | Zhijian | 2005 | 73 |
| | | 2.8 | Pauling Method | Gingerich | 1969 | 43 |
| TiB | | **1.956(16)** | Predissociation Threshold | | 2021 | This work |
| | $^6\Delta$ | 1.81 | MRCI+Q | Tzeli and Mavridis | 2008 | 37 |
| | $^6\Delta$ | 2.36 | B3LYP | Zhijian | 2005 | 73 |
| | | < 3.1 | Pauling Method | Gingerich | 1969 | 43 |
| VB | | **2.150(16)** | Predissociation Threshold | | 2021 | This work |
| | $^7\Sigma^+$ | 2.01 | MRCI+Q | Tzeli and Mavridis | 2008 | 37 |
| | $^7\Sigma^+$ | 2.13 | B3LYP | Zhijian | 2005 | 73 |

[a] Experimentally derived quantities are **bolded**; Quantities from computational or other methods are given in plain text.

Table 2. Previous Studies of YB, ZrB, and NbB. [a]

| Mole-cule | Ground Term | $D_0$ (eV) | Methods | Authors | Year | Reference |
|---|---|---|---|---|---|---|
| YB | $^5\Sigma^-$ S = 2 | **2.057(3)** | Predissociation Threshold | | 2021 | This work |
| | | 1.96 | B97-1 | | 2021 | This work |
| | | 2.17[b] | B3LYP | Kharat *et al.* | 2008 | 40 |
| | | 2.99 | Pauling Method | Gingerich | 1969 | 43 |
| ZrB | $^6\Delta$ S = 2.5 | **2.573(5)** | Predissociation Threshold | | 2021 | This work |
| | | 2.61 | B97-1 | | 2021 | This work |
| | | 3.92[b] | B3LYP | Kharat *et al.* | 2008 | 40 |
| NbB | $^5\Pi/^5\Phi$ S = 1 | **2.989(12)** | Predissociation Threshold | | 2021 | This work |
| | | 3.07 | B97-1 | | 2021 | This work |
| | | 3.40[b] | B3LYP | Kharat *et al.* | 2008 | 40 |

[a] Experimentally derived quantities are **bolded**; Quantities from computational or other methods are given in plain text.

[b] The authors reported a "binding energy" which is ambiguous as to whether $D_e$ or $D_0$ was calculated.

Table 3. Previous Studies of LaB, HfB, TaB, and WB. [a]

| Molecule | Ground Term | $D_0$ (eV) | Methods | Authors | Year | Reference |
|---|---|---|---|---|---|---|
| LaB | | **2.086(18)** | Predissociation Threshold | | 2021 | This work |
| | $^5\Sigma^-$ | 2.54 | B97-1 | | 2021 | This work |
| | S = 2 | 4.16[b] | Diffusion Monte Carlo | Elkahwagy *et al.* | 2018 | 46 |
| | $^5\Sigma^-$ | 2.49[c] | B3LYP | Kalamse *et al.* | 2010 | 41 |
| | | 3.51 | Pauling Method | Gingerich | 1969 | 43 |
| HfB | | **2.593(3)** | Predissociation Threshold | | 2021 | This work |
| | $^4\Sigma^-$ | 2.60 | B97-1 | | 2021 | This work |
| | $^4\Sigma^-$ | 2.70[c] | B3LYP | Kalamse *et al.* | 2010 | 41 |
| TaB | | **2.700(3)** | Predissociation Threshold | | 2021 | This work |
| | $^5\Delta$ | 2.95 | B97-1 | | 2021 | This work |
| | $^3\Sigma^+$ | 2.49[c] | B3LYP | Kalamse *et al.* | 2010 | 41 |
| WB | | **2.730(4)** | Predissociation Threshold | | 2021 | This work |
| | $^6\Sigma^+$ | 2.89 | B97-1 | | 2021 | This work |
| | $^6\Sigma^-$ | 2.77[c] | B3LYP | Kalamse *et al.* | 2010 | 41 |

[a] Experimentally derived quantities are **bolded**; Quantities from computational or other methods are given in plain text.

[b] The authors only reported a value for the $D_e$ of LaB.

[c] The authors reported a "binding energy" which is ambiguous as to whether $D_e$ or $D_0$ was calculated.

Table 4. Derived enthalpies of formations at 0 K for the early MB's. [a]

| $\Delta_f H_{0K}°$ (kJ/mol) | | B |
|---|---|---|
| | | **555(12)** [c] |
| Sc | **376.1(4.2)** [b] | 765.1(14.0) |
| Ti | **470.9(17.0)** [c] | 837.2(20.9) |
| V | **510.9(1.0)** [b] | 858.5(12.1) |
| Y | **423.8(4.2)** [b] | 780.3(12.7) |
| Zr | **607.5(4.2)** [b] | 914.2(12.7) |
| Nb | **718.2(4.2)** [b] | 984.8(12.8) |
| La | **431.3(4.2)** [b] | 785.0(12.8) |
| Hf | **618.9(4.2)** [b] | 923.7(12.7) |
| Ta | **781.0(2.5)** [b] | 1075.5(12.3) |
| W | **848.1(4.2)** [b] | 1139.7(12.7) |

[a] Table entries in **bold** are the enthalpies of formation for the atomic constituents of the early MB's. The entries in plain text are enthalpies of formation derived from Eqn. 1.2.

[b] From Ref. 92

[c] From Ref. 93

Table 5. Measured and calculated properties of the early transition metal borides.

| Molecule | BDE (eV) [a] | BDE (calc) (eV) | $r_e$(Å) | $\omega_e$($cm^{-1}$) | Ground Term | Ground Configuration[b] |
|---|---|---|---|---|---|---|
| ScB | 1.72(6) | 1.79[c] | 2.094[c] | 603[c] | $^5\Sigma^-$ [c] | $2\sigma^1\ 3\sigma^1\ 1\pi^2$ |
| TiB | 1.956(16) | 1.81[c] | 2.080[c] | 583[c] | $^6\Delta$ [c] | $2\sigma^1\ 3\sigma^1\ 1\pi^2\ 1\delta^1$ |
| VB | 2.150(16) | 2.01[c] | 2.043[c] | 585[c] | $^7\Sigma^+$ [c] | $2\sigma^1\ 3\sigma^1\ 1\pi^2\ 1\delta^2$ |
| YB | 2.057(3) | 1.96[d] | 2.306[d] | 517[d] | $^5\Sigma^-$ [d] | $2\sigma^1\ 3\sigma^1\ 1\pi^2$ |
| ZrB | 2.573(5) | 2.61[d] | 2.159[d] | 610[d] | $^6\Delta$ [d] | $2\sigma^1\ 3\sigma^1\ 1\pi^2\ 1\delta^1$ |
| NbB | 2.989(12) | 3.07[d] | 1.988[d] | 698[d] | $^5\Pi/^5\Phi$ [d] | $2\sigma^1\ 3\sigma^1\ 1\pi^3\ 1\delta^1$ |
| LaB | 2.086(18) | 2.54[d] | 2.372[d] | 521[d] | $^5\Sigma^-$ [d] | $2\sigma^1\ 3\sigma^1\ 1\pi^2$ |
| HfB | 2.593(3) | 2.60[d] | 2.128[d] | 584[d] | $^4\Sigma^-$ [d] | $2\sigma^1\ 3\sigma^2\ 1\pi^2$ |
| TaB | 2.700(3) | 2.95[d] | 2.085[d] | 754[d] | $^5\Delta$ [d, e] | $2\sigma^1\ 3\sigma^2\ 1\pi^2\ 1\delta^1$ |
| WB | 2.730(4) | 2.89[d] | 1.891[d] | 730[d] | $^6\Sigma^+$ [d, f] | $2\sigma^1\ 3\sigma^2\ 1\pi^2\ 1\delta^2$ |

[a] Measured in this work.

[b] In all of the ground configurations, the 1σ orbital is doubly occupied.

[c] From Ref. 37

[d] Obtained from calculations for the present study. See Section III for details on methods used.

[e] For TaB, a TD-DFT calculation indicates that a $^3\Pi$ state deriving from the $1\sigma^2\ 2\sigma^1\ 3\sigma^2\ 1\pi^3$ configuration has a vertical excitation energy of 0.072 eV above the $^5\Delta$ ground state. In a more sophisticated calculation, this $^3\Pi$ state could emerge as the ground state.

[f] For WB, a TD-DFT calculation indicates that a $^6\Pi$ state deriving from the $1\sigma^2\ 2\sigma^1\ 3\sigma^1\ 1\pi^3\ 1\delta^2$ configuration has a vertical excitation energy of 0.193 eV above the $^6\Sigma^+$ ground state. In a more sophisticated calculation, this $^6\Pi$ state could emerge as the ground state.

Table 6. The bond dissociation energies, ground states, and ground configurations of the transition metal boride diatomics. [a]

| **ScB**[b] | **TiB**[b] | **VB**[b] | **CrB**[c] | **MnB**[c] | **FeB**[d] | **CoB**[e] | **NiB**[f] | **CuB**[c] |
|---|---|---|---|---|---|---|---|---|
| 1.72(6) | 1.956(16) | 2.150(16) | [1.33] | [0.83] | 2.43(2) | 2.954(3) | 3.431(4) | [2.10] |
| $[^5\Sigma^-]$ | $[^6\Delta]$ | $[^7\Sigma^+]$ | $[^6\Sigma^+]$ | $[^5\Pi]$ | $[^4\Sigma^-]$ | $^3\Delta_3$ | $^2\Sigma^+$ | $[^1\Sigma^+]$ |
| $[2\sigma^1 3\sigma^1 1\pi^2]$ | $[2\sigma^1 3\sigma^1 1\pi^2 1\delta^1]$ | $[2\sigma^1 3\sigma^1 1\pi^2 1\delta^2]$ | $[2\sigma^2 3\sigma^1 1\pi^2 1\delta^2]$ | $[2\sigma^2 3\sigma^1 1\pi^3 1\delta^2]$ | $[2\sigma^2 3\sigma^1 1\pi^4 1\delta^2]$ | $2\sigma^2 3\sigma^1 1\pi^4 1\delta^3$ | $2\sigma^2 3\sigma^1 1\pi^4 1\delta^4$ | $[2\sigma^2 3\sigma^2 1\pi^4 1\delta^4]$ |
| **YB**[g] | **ZrB**[g] | **NbB**[g] | **MoB**[h] | **TcB**[g] | **RuB**[i] | **RhB**[j] | **PdB**[k] | **AgB**[l] |
| 2.057(3) | 2.573(5) | 2.989(12) | [2.18] | [3.31] | 4.815(3) | 5.252(3) | 3.37(22) | [1.51] |
| $[^5\Sigma^-]$ | $[^6\Delta]$ | $[^5\Pi/^5\Phi]$ | $[^6\Pi]$ | $[^5\Sigma^-]$ | $^2\Delta_{5/2}$ | $^1\Sigma^+$ | $^2\Sigma^+$ | $[^1\Sigma^+]$ |
| $[2\sigma^1 3\sigma^1 1\pi^2]$ | $[2\sigma^1 3\sigma^1 1\pi^2 1\delta^1]$ | $[2\sigma^1 3\sigma^1 1\pi^3 1\delta^1]$ | $[2\sigma^1 3\sigma^1 1\pi^3 1\delta^2]$ | $[2\sigma^1 3\sigma^1 1\pi^4 1\delta^2]$ | $2\sigma^2 3\sigma^0 1\pi^4 1\delta^3$ | $2\sigma^2 3\sigma^0 1\pi^4 1\delta^4$ | $2\sigma^2 3\sigma^1 1\pi^4 1\delta^4$ | $[2\sigma^2 3\sigma^2 1\pi^4 1\delta^4]$ |
| **LaB**[g] | **HfB**[g] | **TaB**[g] | **WB**[g] | **ReB**[m] | **OsB**[n] | **IrB**[o] | **PtB**[p] | **AuB**[q] |
| 2.086(18) | 2.593(3) | 2.700(3) | 2.730(4) | [2.78] | 4.378(3) | 4.928(10) | 5.235(3) | 3.77(11) |
| $[^5\Sigma^-]$ | $[^4\Sigma^-]$ | $[^5\Delta]$ | $[^6\Sigma^+]$ | $[^5\Sigma^-]$ | $[^4\Sigma^-]$ | $^3\Delta_3$ | $^2\Sigma^+$ | $[^1\Sigma^+]$ |
| $[2\sigma^1 3\sigma^1 1\pi^2]$ | $[2\sigma^1 3\sigma^2 1\pi^2]$ | $[2\sigma^1 3\sigma^2 1\pi^2 1\delta^1]$ | $[2\sigma^1 3\sigma^2 1\pi^2 1\delta^2]$ | $[2\sigma^1 3\sigma^1 1\pi^4 1\delta^2]$ | $[2\sigma^2 3\sigma^1 1\pi^4 1\delta^2]$ | $2\sigma^2 3\sigma^1 1\pi^4 1\delta^3$ | $2\sigma^2 3\sigma^1 1\pi^4 1\delta^4$ | $[2\sigma^2 3\sigma^2 1\pi^4 1\delta^4]$ |

[a] Quantities in square brackets were obtained in quantum chemical calculations. Underneath each MB, the first line is the BDE in eV, followed by the ground state term symbol and the ground electronic configuration. The ground electronic configurations omit the 1σ orbital, which is always doubly occupied in these molecules.

[b] BDE from this work. Term and configuration from Ref. 37

[c] BDE, term, and configuration from Ref. 37

[d] BDE from Ref. 9 Term and configuration from Ref. 37

[e] BDE from Ref. 9 Term and configuration from Ref. 69

[f] BDE from Ref. 9 Term and configuration from Ref. 94

[g] BDE, term, and configuration from this work.

[h] BDE, term, and configuration from Ref. 38

[i] BDE from Ref. 9 Term and configuration from Ref. 83

[j] BDE from Ref. 9 Term and configuration from Ref. 81

[k] BDE from Ref. 91 Term and configuration from Ref. 95

[l] BDE, term, and configuration from Ref. 96

[m] BDE, term, and configuration from Ref. 39

[n] BDE, term, and configuration from Ref. 9

[o] BDE from Ref. 9 Term and configuration from Ref. 97

[p] BDE from Ref. 9 Term and configuration from Ref. 98

[q] BDE from Ref. 99 Term and configuration from Ref. 96

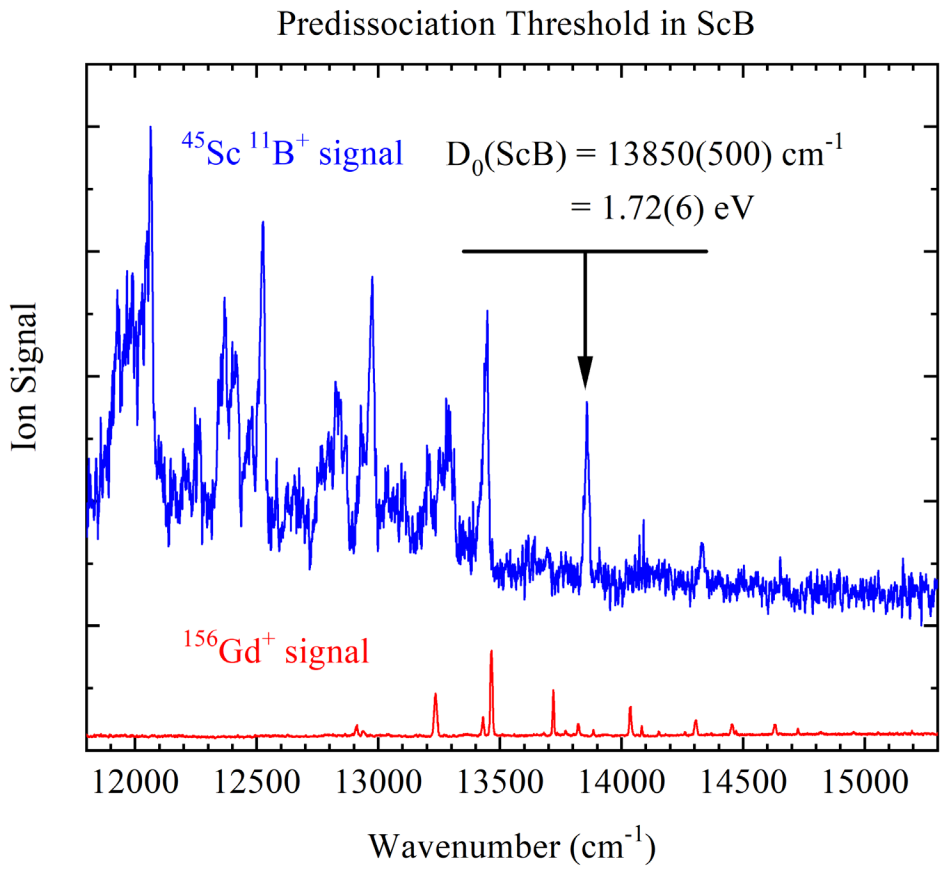


Figure 1. R2PI Spectrum of ScB (upper trace) with its predissociation threshold at 13 850(500) $cm^{-1}$. The atomic spectrum of Gd (lower trace) was used for calibration.

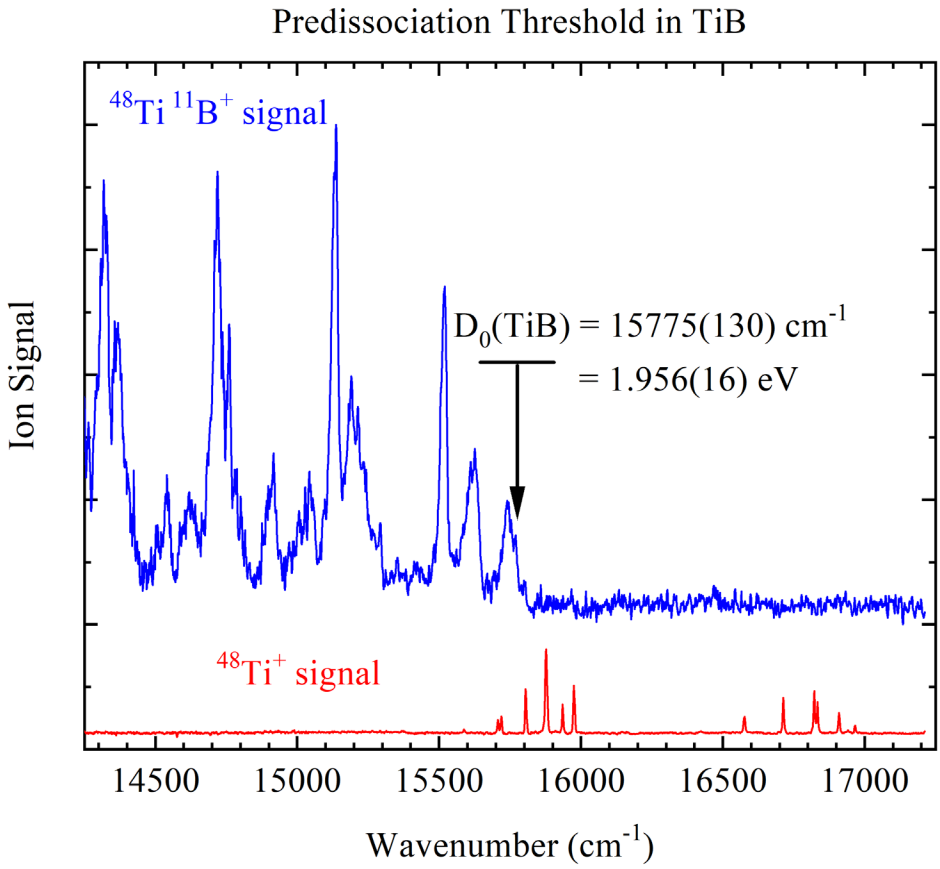


Figure 2. R2PI Spectrum of TiB (upper trace) with its predissociation threshold at 15 775(130) cm$^{-1}$. The atomic spectrum of Ti (lower trace) was used for calibration.

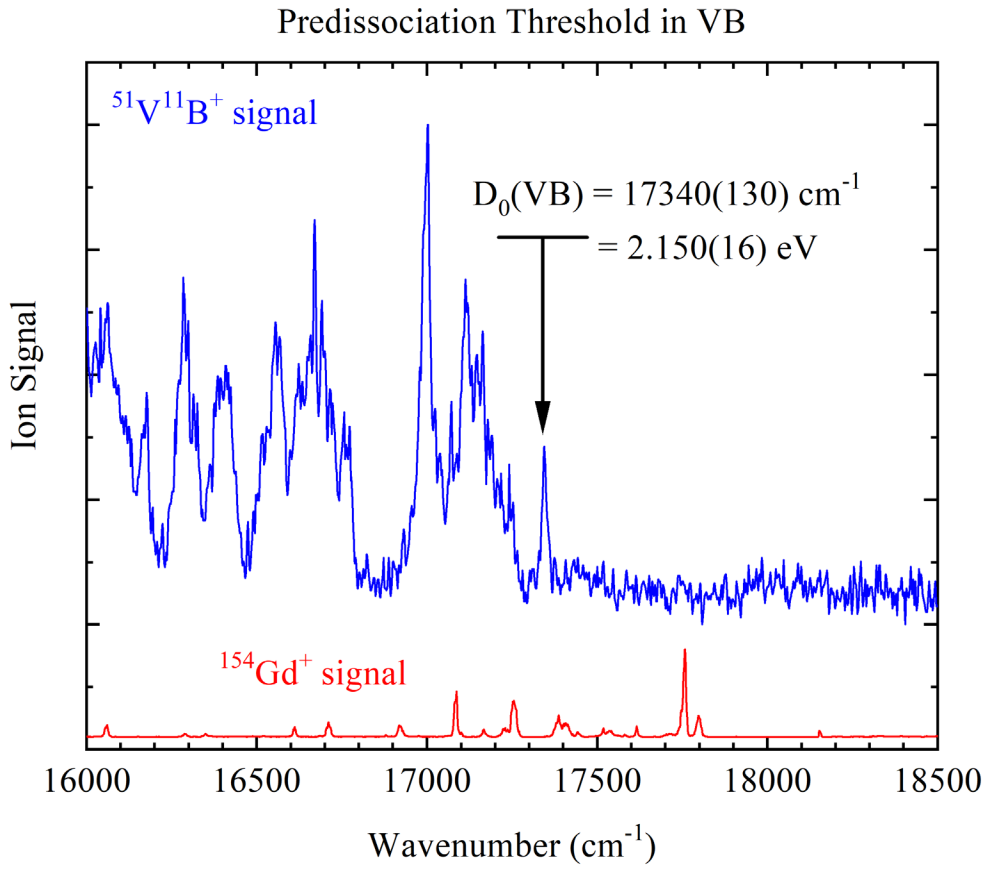


Figure 3. R2PI Spectrum of VB (upper trace) with its predissociation threshold at 17 340(130) cm$^{-1}$. The atomic spectrum of Gd (lower trace) was used for calibration.

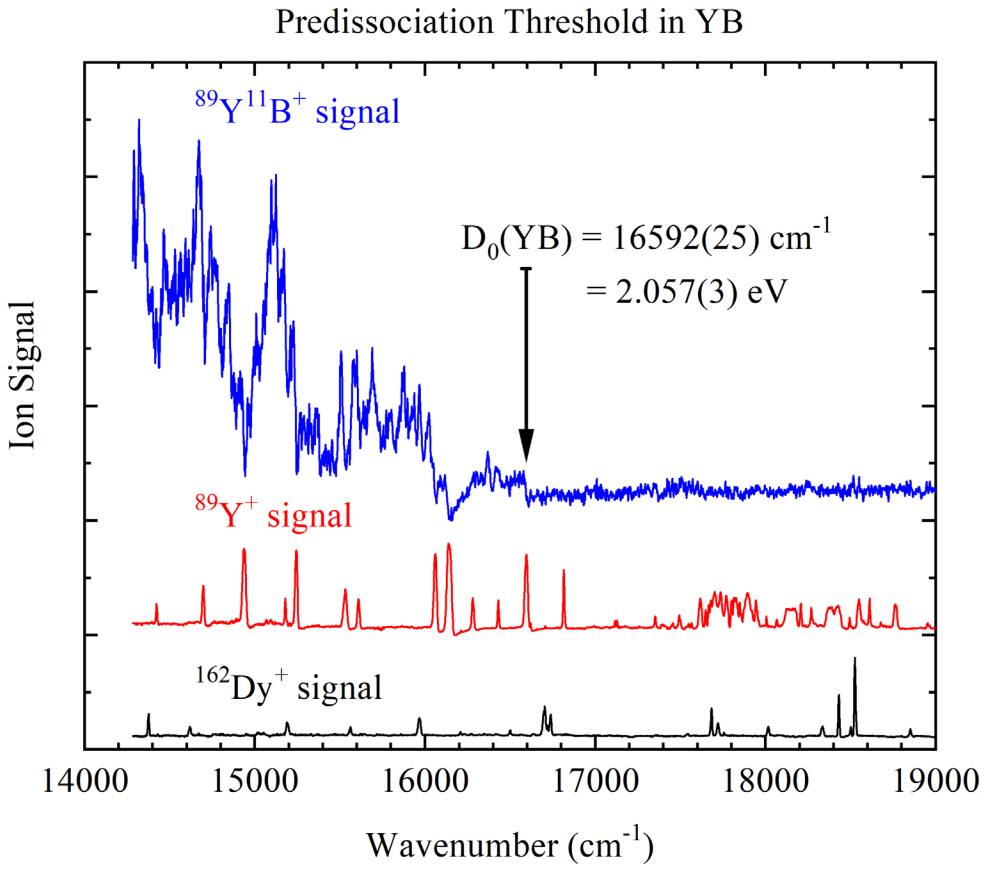


Figure 4. R2PI Spectrum of YB (upper trace) with its predissociation threshold at 16 592(25) cm$^{-1}$. The atomic spectra of Y (middle trace) and Dy (bottom trace) were used for calibration. The sharp drop in $YB^+$ signal at 16 146 cm$^{-1}$ is due to the intense Y atomic transition at this wavenumber, which causes all ion signal to drop at this value due to strong space charge effects.

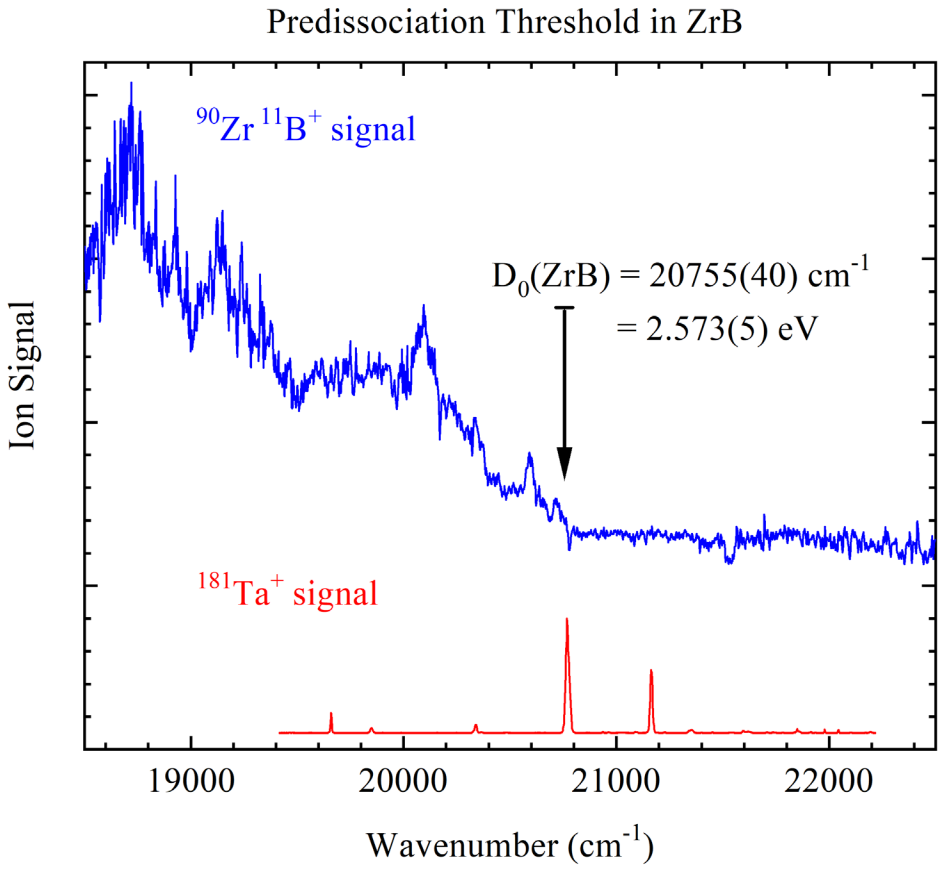


Figure 5. R2PI Spectrum of ZrB (upper trace) with its predissociation threshold at 20 755(40) $cm^{-1}$. The atomic spectrum of Ta (lower trace) was used for calibration.

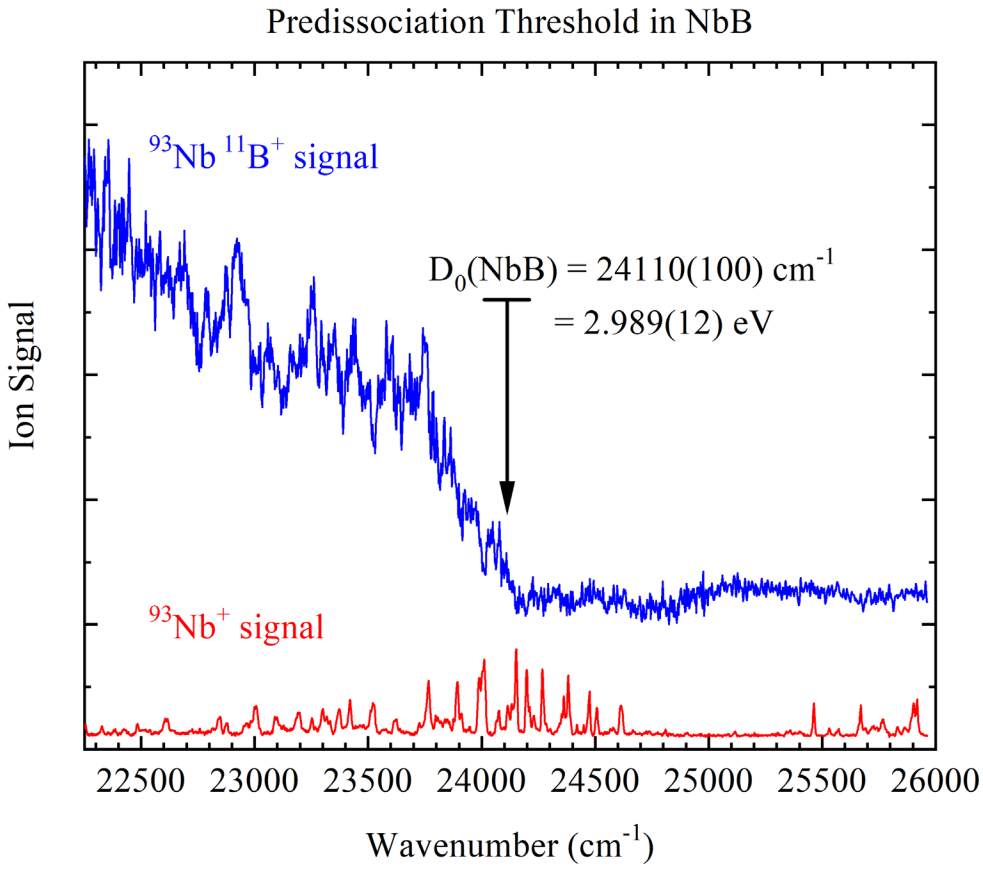


Figure 6. R2PI Spectrum of NbB (upper trace) with its predissociation threshold at 24 110(100) $cm^{-1}$. The atomic spectrum of Nb (lower trace) was used for calibration.

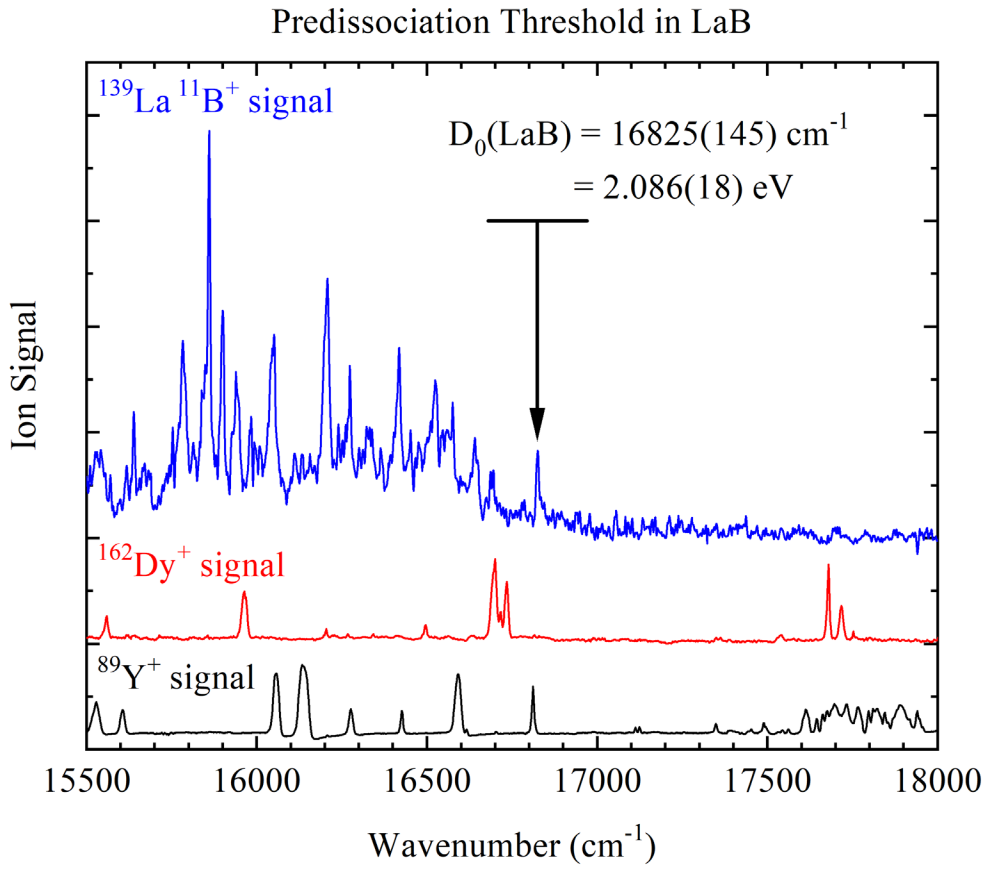


Figure 7. R2PI Spectrum of LaB (upper trace) with its predissociation threshold at 16 825(145) $cm^{-1}$. The atomic spectra of Dy (middle trace) and Y (bottom trace) were used for calibration.

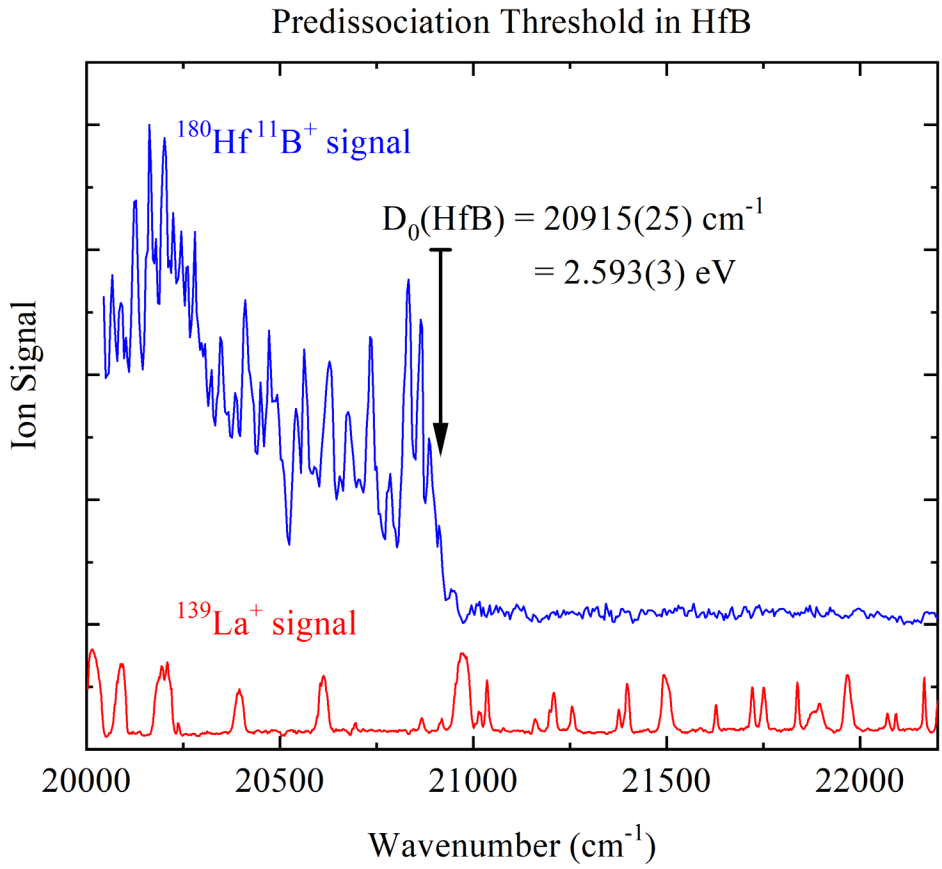


Figure 8. R2PI Spectrum of HfB (upper trace) with its predissociation threshold at 20 915(25) cm$^{-1}$. The atomic spectrum of La (lower trace) was used for calibration.

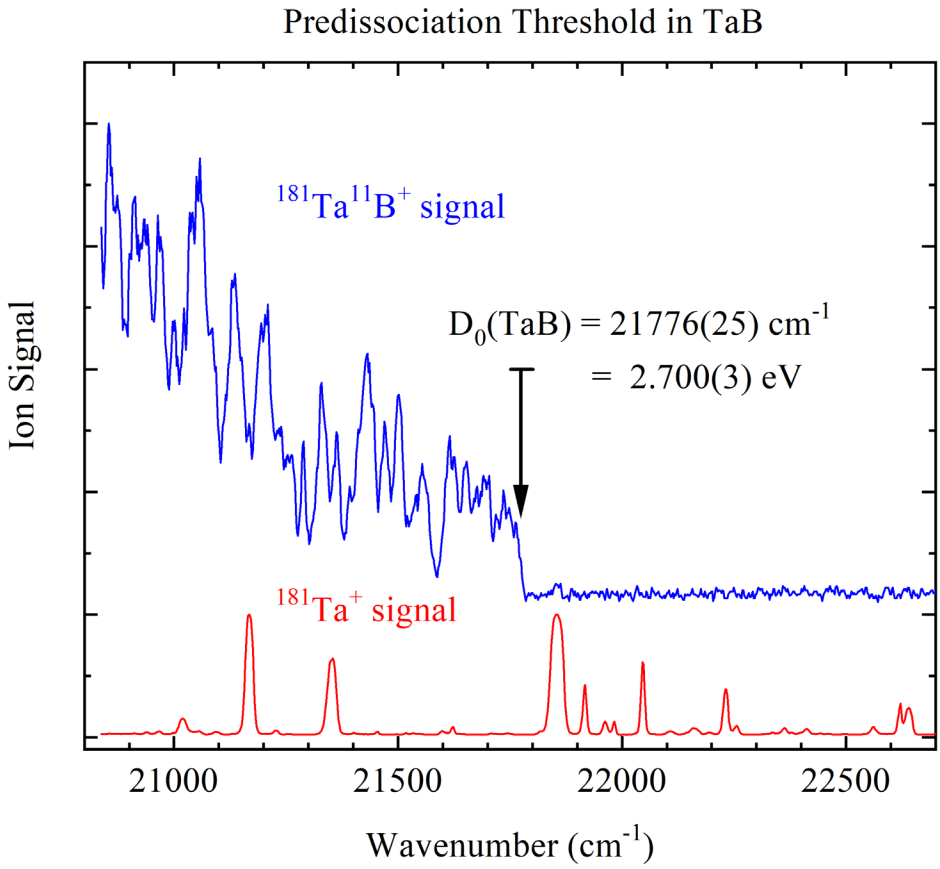


Figure 9. R2PI Spectrum of TaB (upper trace) with its predissociation threshold at 21 776(25) cm$^{-1}$. The atomic spectrum of Ta (lower trace) was used for calibration.

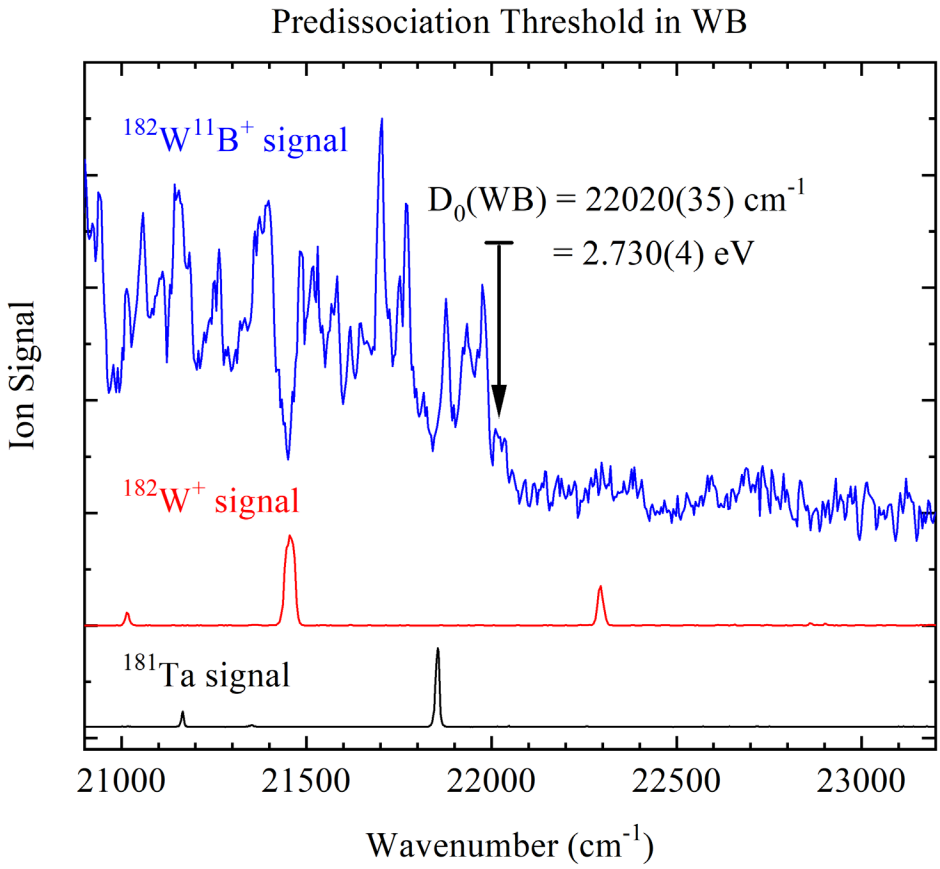


Figure 10. R2PI Spectrum of WB (upper trace) with its predissociation threshold at 22 020(35) $cm^{-1}$. The atomic spectra of W (middle trace) and Ta (lower trace) were used for calibration.

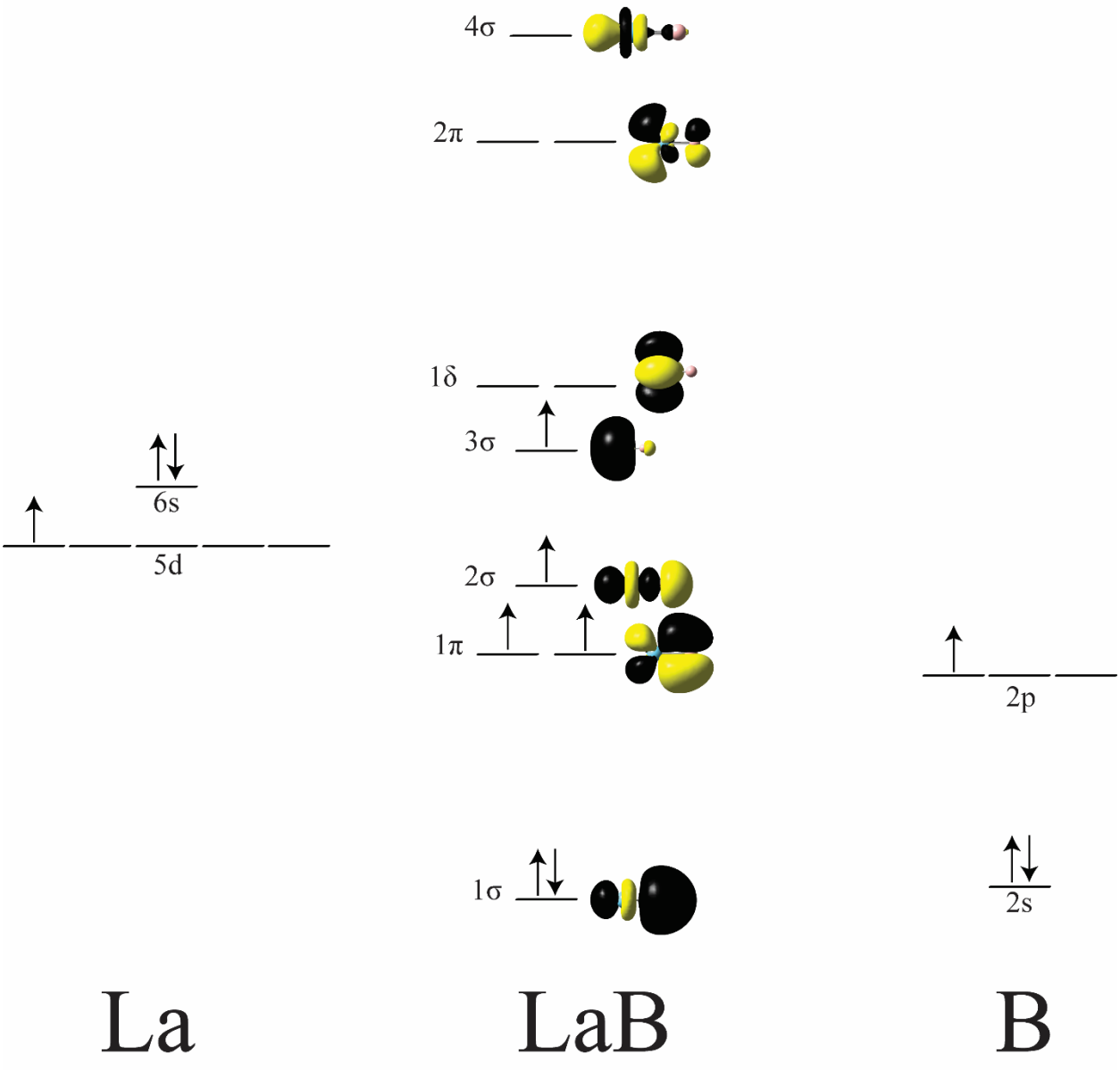


Figure 11. Qualitative depiction of the molecular orbital diagram for the early MB molecules, demonstrated with LaB and its predicted $^{5}\Sigma^{-}$ ground electronic state. Computational details on the generation of this MO diagram are provided in Section III.

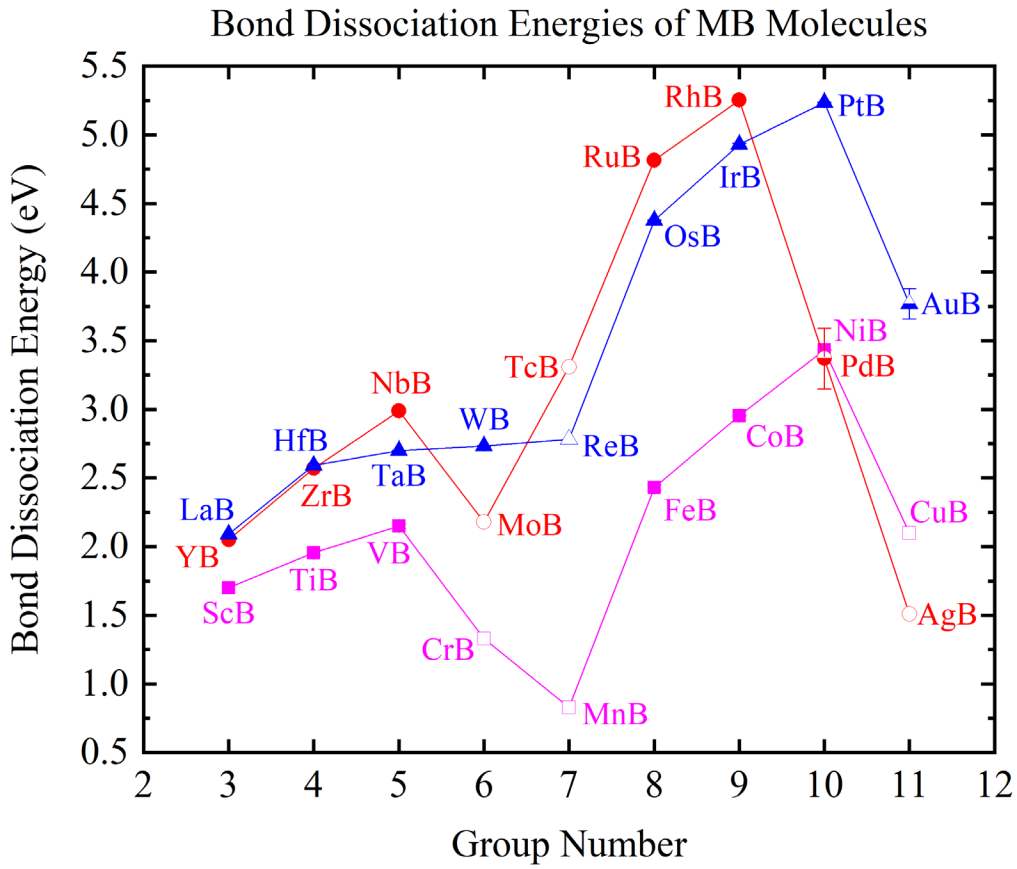


Figure 12. The periodic trends of the BDEs of the transition metal borides. Filled symbols represent BDEs that were assigned from a predissociation threshold using R2PI spectroscopy: magenta squares for the 3d period, red circles for the 4d period, and blue triangles for the 5d period. Half-filled symbols represent BDEs derived from Knudsen Effusion Mass Spectrometry while unfilled symbols represent computed BDEs. References for these values are given in Table 6.

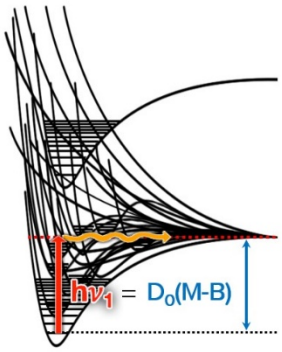


TOC Graphic